NACA

RESEARCH MEMORANDUM

A COMPARISON OF THE AERODYNAMIC CHARACTERISTICS AT TRANSONIC SPEEDS OF FOUR WING-FUSELAGE CONFIGURATIONS AS DETERMINED FROM DIFFERENT TEST TECHNIQUES

By Charles J. Donlan, Boyd C. Myers, II,
and Axel T. Mattson

Langley Aeronautical Laboratory
Langley Air Force Base, Va.

NATIONAL ADVISORY COMMITTEE
FOR AERONAUTICS
WASHINGTON

October 4, 1950
Declassified August 16, 1957

NATIONAL ADVISORY COMMITTEE FOR AERONAUTICS

RESEARCH MEMORANDUM

A COMPARISON OF THE AERODYNAMIC CHARACTERISTICS AT TRANSONIC SPEEDS OF FOUR WING-FUSELAGE CONFIGURATIONS AS DETERMINED FROM DIFFERENT TEST TECHNIQUES

By Charles J. Donlan, Boyd C. Myers, II,
and Axel T. Mattson

SUMMARY

A comparison is made of the high-speed aerodynamic characteristics of a family of four wing-fuselage configurations of 0°, 35°, 45°, and 60° sweepback as determined from transonic-bump model tests in the Langley high-speed 7- by 10-foot tunnel, sting-supported model tests in the Langley 8-foot high-speed tunnel and in the Langley high-speed 7- by 10-foot tunnel, and rocket model tests conducted by the Langley Pilotless Aircraft Research Division. A complementary study of the effect of Mach number gradients and streamline curvature on bump results is also included.

It was found that qualitatively the data obtained from the various test facilities for the wing-fuselage configurations were in essential agreement as regards the relative effects of sweepback and Mach number except for drag at zero lift. Quantitatively, important differences were present. Lift-curve slopes as determined from bump tests tended to be somewhat higher than sting-model data indicated, with consequent differences occurring in drag due to lift. Fuselage-alone drag and wing-fuselage drag as obtained by the bump method were found to be unreliable particularly at Mach numbers above 1.0, but wing-alone drag data were found to be in surprisingly good agreement with available rocket model data throughout the transonic speed range. Aerodynamic-center position as determined from bump data was generally more rearward than sting data indicated, especially for the 60° configuration. Some of this effect has been attributed to the effects of Mach number gradients and flow curvature over the bump. It was evident, however, that for configurations for which aeroelastic effects were important the relative flexibility of the models used in the various facilities accounted for part of the differences in results.

INTRODUCTION

As part of a transonic research program recommended by an NACA Special Subcommittee on Research Problems of Transonic Aircraft Design, a series of wing-fuselage configurations has been investigated in the Langley high-speed 7- by 10-foot tunnel using the transonic-bump method. Publication of these data was expedited despite uncertainties concerning the technique, because it was believed that such data would at least afford qualitative guidance to the aircraft designer. While direct comparison of these data with data obtained by other methods is still limited, recent investigations of several geometrically similar sting-supported models of this series in the Langley 8-foot high-speed tunnel and in the Langley high-speed 7- by 10-foot tunnel permit a comparison of the results at subsonic Mach numbers up to approximately 0.95 and at a supersonic Mach number of 1.2.

The purpose of this paper is to present a comparison of bump data and sting-supported model data for four wing-fuselage configurations of the primary transonic series, corresponding to the 0°, 35°, 45°, and 60° configurations described, respectively, in references 1, 2, 3, and 4. Included in the data for the 45° configuration are some drag comparisons at zero lift obtained from a rocket model investigation conducted by the Langley Pilotless Aircraft Research Division. Some effects of aeroelasticity are also discussed inasmuch as such effects are important in comparing data obtained from different test facilities.

The paper also presents the results of a complementary experimental investigation conducted in the Langley high-speed 7- by 10-foot tunnel to determine the extent to which bump model results are affected by such factors as flow curvature and Mach number gradients.

SYMBOLS

C_L lift coefficient (Twice semispan lift/qS or Total lift/qS)

C_D drag coefficient (Twice semispan drag/qS or Total drag/qS)

ΔC_D total drag coefficient minus drag coefficient at zero lift

C_m pitching-moment coefficient, referred to $0.25\bar{c}$ (Twice semispan pitching moment/$qS\bar{c}$ or Total pitching moment/$qS\bar{c}$)

q effective dynamic pressure over span of model, pounds per square foot $\left(\frac{1}{2}\rho V^2\right)$

S twice wing area of semispan model or wing area of full-span model

$\bar{c}$ mean aerodynamic chord (M.A.C.) of wing based on relationship $\frac{2}{S}\int_0^{b/2} c^2 dy$ (using theoretical tip)

c local wing chord

b twice span of semispan model or span of full-span model

y spanwise distance from plane of symmetry

ρ air density, slugs per cubic foot

V airspeed, feet per second

M effective Mach number over span of model

M_l local Mach number

M_a average chordwise local Mach number

R Reynolds number of wing based on $\bar{c}$

α angle of attack, degrees

L total lift load on wing, pounds

Λ angle of sweepback, relative to $c/4$ line

Λ_l effective sweep angle at any spanwise station, referred to $c/4$

Subscripts:

$L = 0$ at zero lift

m measured value

PART I - BASIC DATA COMPARISON

SCOPE

A comparison is made at several subsonic Mach numbers (0.70, 0.80, 0.85, 0.90, and 0.93) and one supersonic Mach number (approx. 1.2) of the lift, drag, and pitching-moment characteristics of four wing-fuselage combinations of 0°, 35°, 45°, and 60° sweepback as determined from transonic-bump tests of semispan models and sting-supported wind-tunnel models. Most of the transonic-bump data used in the comparison have been taken from published papers (references 1 to 6), although additional bump data for the 0° and 45° configurations obtained subsequent to the original investigations are presented herein for the first time. The wind-tunnel data for the 45° configuration as determined in the Langley 8-foot high-speed tunnel were taken from reference 7. More complete data than that included herein for the other sting-supported wind-tunnel models are being obtained.

For the 45° configuration, a comparison of the drag at zero lift is also made with the results of a rocket model investigation of the same configuration (reference 8).

For the 45° and 60° configurations, static deflection measurements were made for simulated loading conditions and estimated aeroelastic corrections were evaluated for the lift-curve slope and aerodynamic-center position for the bump models and sting-supported models.

REVIEW OF TEST TECHNIQUES

The test techniques employed in obtaining most of the experimental data included in this comparison involve two basic methods: (1) the transonic-bump method employing semispan models and (2) the conventional wind-tunnel method employing full-span sting-supported models. Representative Reynolds numbers for the various testing facilities are given in figure 1. For the most part, only the essential points of the techniques will be reviewed in this section, inasmuch as appropriate references will afford sources for details.

Bump Tests

Method.- The transonic-bump method as used in the Langley high-speed 7- by 10-foot tunnel is described in reference 1. This method of testing involves the placement of a small model in the high-velocity-flow

field generated over a curved surface and is an outgrowth of the NACA wing-flow method (reference 9). Typical contours of local Mach numbers in the vicinity of the model location on the bump are plotted in figure 2(a). Outlines of the $\Lambda = 0^{\circ}$ and $\Lambda = 60^{\circ}$ wings have been superimposed on this diagram in order to illustrate the extent of the spanwise and chordwise gradients in Mach number. In practice, no attempt is made to account for the effects of these gradients apart from evaluating the effective test Mach number on the basis of the relationship

$$M = \frac{2}{S}\int_{0}^{b/2} cM_a \, dy$$

The results of a complementary investigation conducted primarily to study additional effects that Mach number gradients may have on the aerodynamic characteristics as determined from bump tests are discussed in part II of this paper.

The model is attached to an electrical strain-gage balance mounted inside the bump and is so arranged that the gap between the bottom of the fuselage end plate and the bump surface is about 3/64 inch. The chamber containing the balance is sealed and vented to an orifice on the bump such that the static pressure in the chamber is roughly the same as that existing over the bump. A small opening of a size sufficient to allow an angle-of-attack range of about 16° is cut in the vicinity of the wing butt of the model. This opening is covered by the fuselage and its end plate. A photograph of a typical wing-fuselage model configuration mounted on the bump is shown in figure 3(c).

A unique arrangement (fig. 4) is used for measurements of the drag at zero lift in order to minimize leakage and to avoid the use of an end plate. In this arrangement, a foam-rubber wiper seal is attached to the model and rests against the underside of the cover plate and effectively blocks off the small gap (about 1/16 in.) around the root of the wing. The seal pressure must be carefully adjusted to avoid friction effects, but this method, in general, has been found to be more satisfactory for drag determinations than any unsealed arrangement.

Models.- A drawing of the four bump models used in this comparison is given in figure 5. Actually, data are being presented for six bump models, two sets each for the $\Lambda = 0^{\circ}$ and 45° configurations and one set each for $\Lambda = 35^{\circ}$ and 60° configurations. The additional models for the 0° and 45° configurations were constructed for the complementary investigation discussed in part II of this paper. These models were made of steel and hence were stiffer than the original $\Lambda = 0^{\circ}$ and 45° models which were made of beryllium copper. The bump data for these additional tests have been included in the basic comparison, however, because of certain discrepancies in results.

The fuselage used was made of brass and its ordinates are given in table I. It was bent to conform to the bump surface as indicated on figure 5.

The various bump models for which data are presented, as well as the references from which the data were taken, are summarized in the following table:

$\Lambda_{c/4}$ (deg)	Designation	Construction material	Source
0	Model 1 Model 2	Beryllium copper Steel	Reference 1 Unpublished
35	Model 1	Beryllium copper	References 2 and [a]5
45	Model 1 Model 2	Beryllium copper Steel	References 3 and [a]6 Unpublished
60	Model 1	Steel	Reference 4

[a]Since the publication of references 2 and 3, drag at zero lift with the foam-rubber seal was obtained for this model and subsequently published in noted reference.

Corrections.- No jet-boundary corrections have been applied to any of the bump data. Corrections for fuselage base pressure were determined and found to be small. They have not been applied to the data.

Except for the measurements of the drag at zero lift, no tare corrections for the effect of the fuselage end plate or leakage have been applied to other components. Special tests, in which a few models were investigated at several angles of attack while mounted without end plates and with the foam-rubber seal attached, indicated small but inconsistent tare effects on lift, pitching moment, and drag due to lift.

Sting Tests

The sting methods used in the Langley 8-foot high-speed tunnel and the Langley high-speed 7- by 10-foot tunnel are basically similar and will be considered together in the following discussion. Additional details regarding the 8-foot sting method of testing may be found in reference 7.

Method.- The tests were conducted in closed-throat, single-return-type tunnels. In order to minimize interference effects between model and support the models were mounted on a sting which is attached to a supporting structure downstream of the test sections. A view of the models mounted in the tunnels is shown in figure 3. The Langley high-speed 7- by 10-foot-tunnel tests were run at various angles of attack through the Mach number range by employing angle-of-attack couplings, whereas the 8-foot high-speed-tunnel tests were conducted by changing angle of attack at a constant Mach number. The models are attached to internal strain-gage balances.

Models.- A drawing of the sting models together with pertinent dimensions is given in figure 6. The wings were constructed of aluminum alloy except the $\Lambda = 35^{\circ}$ wing in the Langley 8-foot high-speed tunnel and the $\Lambda = 45^{\circ}$ wing in the Langley high-speed 7- by 10-foot tunnel which were made with a steel insert and bismuth-tin filler. The fuselages were hollow and constructed of aluminum for the Langley high-speed 7- by 10-foot-tunnel configuration and of steel for the Langley 8-foot high-speed-tunnel configuration. They were designed by cutting off the rear portion of a body of revolution with a fineness ratio of 12 to form one with a fineness ratio of 10. (See table I.)

Corrections.- The method of reference 10 was used to correct for the effects of the model and its wake on Mach number and dynamic pressure. No corrections due to sting interference, which are believed to be small, have been determined or applied to the data. A representative account of interference effects as well as base-pressure measurements are presented in reference 7 for the 8-foot-tunnel models. Base-pressure corrections to drag were determined at zero angle of attack and have been applied to both the 7- by 10-foot-tunnel data and the 8-foot tunnel data. The drag at zero lift, therefore, corresponds to free-stream static pressure at the base of the fuselage. The correction to the drag coefficient was of the order of 0.002.

Effect of Flexibility

When the angle of sweepback is appreciably increased, the influence of wing flexibility on the aerodynamic characteristics becomes increasingly important. It follows, therefore, that comparisons of aerodynamic data for swept wings from different test facilities become exceedingly difficult because of differences in model construction, methods of mounting, and testing techniques. In order to obtain some idea of the effect of wing model flexibility on the aerodynamic results, two of the 7- by 10-foot-tunnel bump and sting wings ($\Lambda = 45^{\circ}$ and 60°) were loaded with a simulated elliptical-type loading along the quarter-chord line. The angle of attack at several spanwise stations was measured while the models were statically loaded. As an example of the results

obtained, a deflection diagram for the $\Lambda = 60^{\circ}$ sting model is shown in figure 7. Correction factors for the lift-curve slope $\left(C_{L_\alpha}\right)$ and the aerodynamic center $\left(\partial C_m/\partial C_L\right)$ have been evaluated from such diagrams for these wings and are presented in figure 8. The reason the generally weaker sting wings $\left(\Lambda = 45^{\circ}\text{, steel insert; } \Lambda = 60^{\circ}\text{, aluminum}\right)$ have a smaller correction to C_{L_α} than the steel bump wings is attributed directly to the method of support. The 7- by 10-foot-tunnel sting wings are mounted about a point 10 percent semispan outboard of the fuselage center line, whereas the bump wings are mounted about a point inside the bump 25 percent semispan from the fuselage center line.

Inasmuch as the 8-foot-tunnel models are similar in construction and mounting to the 7- by 10-foot-tunnel models, the same correction factors are applicable to the 8-foot-tunnel results.

RESULTS AND DISCUSSION

The results of the basic comparison are summarized in the following figures:

	Figure
Basic wing-fuselage force and moment data:	
$\Lambda = 0^{\circ}$ configuration	9
$\Lambda = 35^{\circ}$ configuration	10
$\Lambda = 45^{\circ}$ configuration	11
$\Lambda = 60^{\circ}$ configuration	12
Zero-lift drag variation with Mach number:	
Bump and sting results for -	
Wing-fuselage, all configurations	13
Fuselage alone	14
Bump, sting, and rocket results for -	
$\Lambda = 45^{\circ}$ configuration	15
Basic aerodynamic parameter comparisons:	
C_{L_α} and $\partial C_m/\partial C_L$ against M	16
Aerodynamic parameter comparisons with estimated aeroelastic corrections applied:	
C_{L_α} and $\partial C_m/\partial C_L$ against M	17

The existence of nonlinear variations of C_L and C_m with α decreases the significance of the comparison of the parameters C_{L_α}

and $\partial C_m/\partial C_L$ because of the difficulty in ascertaining slopes. For the comparisons presented in this paper the slopes were averaged through zero lift over an angle-of-attack range up to an angle at which obvious departures from linearity occurred. Accordingly, the slopes presented in this comparison paper may not be in exact quantitative agreement with those presented in the basic reference reports.

0° Sweep Configuration

Lift.- The variation of lift with angle of attack is approximately the same for all models (fig. 9(a)) although quantitative differences are evident especially at the higher angles of attack. In the lower lift range the sting models exhibit a somewhat more rapid variation of lift-curve slope with Mach number than the bump model, particularly in the vicinity of the force break (fig. 16(a)). Also variations in lift coefficient, especially in the vicinity of $C_{L_{max}}$, are more pronounced for the sting models although the actual values of $C_{L_{max}}$ are in fair agreement. It is perhaps to be expected that the agreement in lift is generally poorest wherever the lift changes are most rapid. Bump model 2 agrees a little better with the sting-mounted data than the original model 1 (reference 1). Some of the factors that are partly responsible for the lack of duplication in bump results are discussed in part II of this paper. In this regard, however, it should be noted that small differences are also evident in the two sets of sting data, particularly in regard to the variation of C_{L_α} with M (fig. 16).

Pitching moment.- For the most part the variations of C_m with C_L (fig. 9(b)), particularly the rapid variation at high values of C_L, are in practical agreement for all models up to Mach numbers at which rapid rearward movement of aerodynamic center occurs (about $M \approx 0.85$ in fig. 16(b)). As regards aerodynamic-center position, the bump models are in good agreement with the 7- by 10-foot-tunnel sting data, whereas the 8-foot-tunnel sting results indicate a more forward aerodynamic-center location at Mach numbers below 0.85. However, above $M = 0.85$ the bump results and the 8-foot-tunnel sting results are in good agreement throughout the subsonic Mach number range as well as in the upper transonic speed range near $M = 1.2$.

Drag.- Drag due to lift (fig. 9(c)) is in good agreement for all models except in the maximum lift range. The lower drags indicated by the 8-foot-tunnel sting model at the higher lift coefficients are a result of the lower angle of attack required to sustain these lift coefficients.

The variation of $C_{D_{L=0}}$ with Mach number for the $\Lambda = 0^{\circ}$ wing-fuselage configurations (fig. 13) appears to be in good agreement, but

the bump models exhibit a considerably higher value of drag throughout the Mach number range than do the sting models. It was the high drag obtained with the bump model in the original investigation (reference 3), even when a sponge wiper seal was used to avoid leakage and end-plate effects, that prompted the construction and investigation of bump model 2. The results of the two bump tests, however, seem to be in excellent agreement. Roughness applied to the bump model wings in an effort to simulate the type of boundary-layer transition likely to occur at a high Reynolds number was of little value for this model and the application of roughness resulted in even higher values of drag.

The high absolute drag obtained with the bump model is attributable, in part, to the high drag obtained with the fuselage alone. Fuselage-alone drag data as obtained by the bump method are compared with fuselage drag data from other sources in figure 14. Not only does the fuselage-alone bump drag appear to be about twice as great as that obtained from wind-tunnel and drop tests (reference 11) but the variation with Mach number above $M = 1.0$ appears to be unreliable. For this reason, the variation of drag with Mach number at Mach numbers in excess of 1.0 for any of the bump wing-fuselage configurations should be used with caution. It is believed that the high fuselage drag is largely a result of the gap between the fuselage and the bump surface inasmuch as the drag caused by the base pressure was found to be small.

35° Sweep Configuration

Lift.- In regard to the variation of lift with angle of attack, the bump results and the 7- by 10-foot-tunnel sting results are in good agreement (fig. 10(a)) and both exhibit higher lift-curve slopes than the 8-foot-tunnel sting model (fig. 16(a)). The differences in lift behavior exhibited by the two sting models in the lower angle-of-attack range are somewhat surprising even when the slight changes in wing sweep angle (2.4°) are considered (fig. 6). The reasons for these discrepancies in lift behavior are not known at present. It is evident also that while the lift variations at the higher lift coefficients are similar for the bump model and the 8-foot-tunnel sting model, the rapid changes in lift for the 8-foot-tunnel sting model are delayed to a higher angle of attack, perhaps because of the higher Reynolds number of the 8-foot-tunnel data.

Pitching moment.- The bump model and the two sting models exhibit similar trends in pitching-moment behavior in the lower lift range but the lift coefficients at which rapid changes in pitching-moment behavior occur are higher for the 8-foot-tunnel sting model (fig. 10(b)). The bump data give an aerodynamic-center position about 5 percent more rearward than the sting models at the lower Mach numbers (fig. 16(b)) and indicate a less rapid rearward movement with Mach number than was

obtained with the 8-foot-tunnel sting model. At supersonic Mach numbers the bump and sting results are in fair quantitative agreement.

Drag.- The drag due to lift (fig. 10(c)) indicates similar trends for all models and reflects the differences in lift behavior previously noted. The variation of $C_{D_{L=0}}$ with M (fig. 13) for the bump model is more rapid below the Mach number for drag rise and less rapid in the vicinity of drag rise than that for the sting models. It is of interest to note, however, that the drag variation obtained with the bump wing-fuselage configuration is similar to that obtained for the bump wing alone (reference 5).

45° Sweep Configuration

Lift.- The lift characteristics of the two sting models are in very good agreement (fig. 11(a)), particularly in regard to the variation of the mean lift-curve slope with Mach number (fig. 16(a)). The 45° configuration is flexible enough to require consideration of aeroelastic effects on lift-curve slope. These corrections have been estimated for the 7- by 10-foot-tunnel sting model and for bump model 2 (fig. 8) and have been applied to the data in figure 17(a). Inasmuch as the 7- by 10-foot-tunnel sting data and the 8-foot-tunnel sting data are in good basic agreement, the corrected values given in figure 17(a) can be assumed to apply to the 8-foot-tunnel data also.

The bump models appear to be in general qualitative agreement with the sting results. It will be noted, however, that the bump models give somewhat higher lift-curve slopes (fig. 16(a)) and indicate a more linear variation of lift with angle of attack in the higher angle-of-attack range (fig. 11(a)).

Pitching moment.- The pitching-moment behavior exhibited by the various models is perplexing (fig. 11(b)). Even the sting models indicate some differences, especially in regard to aerodynamic-center position (fig. 16(b)). The development of an unstable pitching-moment variation at a very low value of C_L for bump model 1 was regarded with suspicion when originally obtained (reference 3), but check tests made at that time produced similar results. Subsequently, bump model 2 was constructed for the bump-wall comparison discussed later in this paper and gave the type of pitching-moment variation shown in figure 11(b). It is evident that for bump model 2, the onset of the unstable pitching-moment variation has been delayed to higher lift coefficients and is in better accord with 8-foot-tunnel sting data in this respect. The aerodynamic center is, however, somewhat more rearward than was obtained for other models (fig. 16(b)). The pitching-moment data in reference 12 indicate that, in the Reynolds number range

of the bump tests, surface conditions can result in a forward movement of the aerodynamic center of several percent; whereas, at the higher Reynolds numbers (greater than 1×10^6), roughness has little effect. It is interesting to note that the application of roughness to the 8-foot-tunnel sting model (reference 7) and to the 7- by 10-foot-tunnel sting model (unpublished) also had little effect on aerodynamic-center position.

The corrections to the aerodynamic-center location attributable to aeroelastic effects (figs. 8 and 17(b)) appear to be rather small for this configuration and are not an important factor in explaining the discrepancies obtained.

Drag.- Drag due to lift (fig. 11(c)) is in good agreement for the two sting models. Bump model 2 is in fair agreement with the sting results, but the originally published drag data for bump model 1 indicate definitely lower drags in certain portions of the lift range, particularly at the lower Mach numbers.

The differences observed in the zero-lift drag variation with Mach number for the two bump models (fig. 13) are probably a result of changes in fuselage drag inasmuch as the wing-alone drag for the two models is in excellent agreement (compare fig. 15 of reference 6 with fig. 21 of this paper). The inconsistencies in these wing-fuselage drag data again emphasize the difficulty encountered in measuring the drag of half-bodies of revolution by the bump method.

A comparison of the drag at zero lift utilizing the results of rocket model tests of the 45° configuration, reference 8, is presented in figure 15. The abnormally high fuselage-alone drag obtained on the bump (fig. 14) makes a comparison in the transonic range difficult even when compared on the basis of wing-fuselage minus fuselage drag. It appears that the bump model does not reflect the peak drag obtained with the rocket configuration in the vicinity of $M = 0.98$. This peak drag has been traced to interference effects between the wing and fuselage (reference 8). Inasmuch as the fuselage-alone drag is considered questionable from bump tests, it is not surprising that such interference effects are not observed in the bump data.

60° Sweep Configuration

Lift.- The lift characteristics are in essential agreement (fig. 12(a)) although the bump model fails to reveal the nonlinearities exhibited by the sting models at the low angles of attack. This fact is perhaps responsible for the slightly higher values of lift-curve slope obtained for the bump model (fig. 16(a)). The corrections for flexibility

do not appreciably affect the comparison in regard to lift-curve slope (figs. 8 and 17(a)).

Pitching moment.- It is the pitching-moment behavior of the 60° configuration that exhibits the largest discrepancies encountered in this comparison. The sting models are in fair agreement at the higher angles of attack (fig. 12(b)) but exhibit different pitching-moment slopes in the lower lift range (fig. 16(b)). These differences are small, however, compared to the extremely rearward aerodynamic-center position indicated from bump data. The bump data also indicate unstable pitching moments occurring at considerably lower lift coefficients than the sting models. This result does not appear to be a sole consequence of the low Reynolds number of the bump tests inasmuch as unpublished tests of the 7- by 10-foot sting model in the Langley 300 MPH 7- by 10-foot tunnel at a Reynolds number of about 500,000 indicated similar characteristics to those shown for the 7- by 10-foot sting model at $M = 0.7$.

It is believed that the indicated differences for the sting models at the low lift coefficients may not really be present. It was necessary to fair the 8-foot sting data with considerably fewer points than were available for the 7- by 10-foot sting data, and wherever nonlinear variations occur a great many points are necessary to define the character of the nonlinearity. Essentially, therefore, the sting data are in good agreement and the important feature of the comparison is found in the considerably more rearward aerodynamic-center position obtained with the bump model. A considerable portion of the discrepancy in aerodynamic-center location is attributable to the larger aeroelastic effects experienced by the sting model (fig. 8). The estimated effect of the wing flexibility on the sting model results was to move the aerodynamic-center appreciably rearward as shown in figures 16(b) and 17(b). It will be noted, however, that the flexibility for the bump model is rather small and that the aerodynamic center indicated for the bump model is still considerably more rearward than for the sting model even when the flexibility of both models is considered.

It is believed that the more rearward aerodynamic-center location obtained on the bump model for highly swept wings is also closely related to the effect of the bump curvature. For the 60° bump model the spanwise variation of sweep angle due to the curvature of flow is shown in figure 18. Thus, the root sections are operated in excess of 60° whereas the tip sections are operated at sweep angles of less than 60°. The effect of this sweep variation on the span loading has been estimated and it has been determined that, although the effect of this sweep variation on lift-curve slope was small, the aerodynamic-center position was moved about 5 percent of the mean aerodynamic chord rearward. This correction has been noted on figure 17(b) for $M = 0.7$ and it is seen that much of the discrepancy in the pitching-moment

slope existing between the sting and bump results at this Mach number appears to be accounted for. Although it is realized that these factors may not be entirely responsible for all the discrepancies attributed to them, the indications are that: (1) highly swept models tested on the bump used in this comparison are apt to result in considerably further rearward movements of the aerodynamic center than would be anticipated and that (2) large differences in aeroelastic effects can appreciably modify comparisons of data obtained in different test facilities.

Drag.- Drag due to lift is in fair agreement (fig. 12(c)) but the drag at zero lift (fig. 13) is considerably higher in absolute magnitude for the bump model than that obtained on either of the sting models, although the results do exhibit the very small variation with Mach number that would be expected for this wing.

General Remarks on Data Comparison

Despite the differences that have been noted in the comparison of the separate configurations, a cross-comparison of the data for the 0°, 35°, 45°, and 60° configurations indicates that the bump model results exhibit about the same qualitative effects of sweepback and Mach number on the aerodynamic characteristics of the wing family except for drag at zero lift. Important quantitative difference in the results are evident, however. In general, wherever sudden changes in lift, drag, and pitching moment occurred, the bump model results indicated less rapid changes with Mach number and angle of attack than the sting model results. (See, for example, figs. 9, 13, 16, and 17.) The bump data generally resulted in higher lift-curve slopes than were obtained from sting data, and the variation of lift-curve slope with Mach number was less rapid than sting data indicated. Drag at zero lift as obtained from the bump data for the wing-fuselage combinations and for the fuselage alone does not appear to be reliable as regards either the absolute value of drag or the rate of drag increase with Mach number in the neighborhood of the drag rise Mach number. It will be shown subsequently in this paper that this result is largely attributable to fuselage drag results. On the other hand, drag due to lift was generally in fair agreement for the bump and sting models except where discrepancies existed in the angle of attack required to support the same lift. The position of the aerodynamic center as determined from bump tests appears to be more rearward than sting model data indicate, especially at the higher sweep angles, but differences in the flexibility of the models used make comparisons of aerodynamic-center position difficult because of aeroelastic effects.

Although distinguishing trends are evident in the data, the results of a comparison of only four models do not permit detailed conclusions to be drawn regarding the reliability of bump data in general. It appears almost essential to examine each model individually because of the many factors involved in comparing the results obtained from one technique with those of another.

General Remarks on Test Methods

In comparing the results obtained with similar models in different test facilities, it is usually not possible to control test conditions closely enough so that differences in results can be attributed to a unique factor. A list of some of the factors that must be considered in evaluating the results obtained by various test methods would include the following items:

1. Mach number gradients
   (a) Spanwise
   (b) Chordwise

2. Flow curvature

3. Boundary layer at model
4. Flow leakage about model
5. End-plate conditions

   } Reflection-plane technique

6. Flow steadiness

7. Humidity conditions

8. Reynolds number of test

9. Accuracy of model construction

10. Flexibility of model

All of these items are perhaps not of equal importance for all test methods, but each test method must be examined for those factors most likely to influence the results obtained by that method. Thus, it is evident from the Mach number gradients shown in figure 2(a) that items 1 and 2 constitute important defects in the bump method of testing, at least for the particular bump referred to in this paper. Items 3, 4, and 5 are important considerations for any method utilizing the reflection-plane technique and perhaps assumed more critical roles in bump testing because of the presence of items 1 and 2. Items 6, 7, 8, 9, and 10 are important considerations in any test method. Little is known concerning the effects of flow steadiness, item 6. Humidity conditions, item 7, are not believed to be an important factor in the comparison presented in this paper because of the elevated temperatures at which the wind tunnels were operated (reference 7). The low Reynolds number of bump tests, item 8, has always been considered one of the major deficiencies of this method of testing (fig. 1). Accuracy of model construction, item 9, becomes relatively more important in bump

investigations because the small size of the models requires precision workmanship not only in regard to constructing models but in positioning them for tests.

It has not been possible to control test conditions on the bump closely enough to permit isolation of the influence of the many factors involved. It has been possible, however, to examine the importance of Mach number gradients and flow curvature (items 1 and 2) by investigating the bump models on a reflection plane in the Langley high-speed 7- by 10-foot tunnel. The test conditions for this arrangement were practically the same as the bump test conditions except that there was no flow curvature and relatively small Mach number gradients compared to the bump. It was not possible, however, to obtain as high Mach numbers with this arrangement as was possible with the bump method.

An investigation to examine the effects of Mach number gradients and flow curvature on the bump results is described in the following section.

PART II - EFFECTS OF MACH NUMBER GRADIENTS AND FLOW CURVATURE ON BUMP RESULTS

DESCRIPTION OF WALL REFLECTION-PLANE TECHNIQUE

Models and method.- The two models that were used in the bump-wall investigation were the 0° and 45° models shown in figure 5. The wings of these models were of steel and were especially constructed for this investigation. The models were tested on the bump and on the wall plate as wings alone and in combination with the fuselage. Figure 3(d) shows one of the models mounted on the reflection plate. The plate was fastened to the wall of the Langley high-speed 7- by 10-foot tunnel and was located so as to bypass the tunnel boundary layer. The length of the plate was such that the boundary layer at the model position was approximately the same as that existing at the model location on the bump. Every effort was made to make the wall and bump installation similar by duplicating details such as mounting brackets, end-plate, and gap conditions. For the wall tests, the fuselage was not curved as shown in figure 5.

Test conditions.- The velocity field in the vicinity of the models is shown in figure 2(b). For the Mach numbers indicated, it is evident that the velocity gradients are very much less than those occurring on

the bump at similar Mach numbers and are principally chordwise gradients, whereas the bump gradients are predominantly spanwise. For Mach numbers below $M = 0.95$, the flow field was essentially free of any velocity gradients. The wall reflection-plane method is essentially the same as the bump method. The main tunnel flow remains subsonic for all test Mach numbers below $M = 1.08$ at which value a Mach number of 1.0 is obtained on the opposite wall from the plate. By testing these models on the wall plate, it was hoped that most of the itemized factors would be duplicated in the wall and bump tests except items 1 and 2. Actually, it was not possible to achieve this end completely. Nevertheless, it was believed that by having the same Reynolds number for both tests (see fig. 1), one of the principal uncertainties in the data comparison would be eliminated.

RESULTS AND DISCUSSION

A comparison of the results obtained by the wall reflection-plane method and the bump method is contained in the following figures:

	Figure
Wing-alone and wing-fuselage characteristics:	
$\Lambda = 0^{\circ}$ configuration	19
$\Lambda = 45^{\circ}$ configuration	20
Variation of drag at zero lift with Mach number	21
C_{L_α} and $\partial C_m/\partial C_L$ against M:	
$\Lambda = 0^{\circ}$	22(a)
$\Lambda = 45^{\circ}$	22(b)
Comparison with 8-foot sting data	23

The bump data presented in the preceding figures are the same as that presented for bump model 2 in figures 9 and 11.

0° Sweep Configuration

Lift.- Similar trends in the over-all variation of lift with angle of attack are evident (fig. 19(a)) although bump data consistently indicate a somewhat less rapid variation of lift at the angles of attack near $C_{L_{max}}$. It has been noted previously (fig. 9(a)) that this wing appears to be particularly sensitive at the high angles of attack, so that differences in results between the bump and wall tests in this angle-of-attack range are not too surprising.

For the wing alone, the lift-curve slopes as determined from wall data (fig. 22(a)) are in excellent agreement with theoretical values determined from reference 13. It will be noted, however, that the lift-curve slopes for both the wing and wing-fuselage configurations as determined from bump data are somewhat higher than the values determined from the wall data.

Pitching-moment.- The pitching-moment characteristics are in good qualitative agreement, particularly for the wing-fuselage configuration and especially as regards the lift coefficient at which rapid changes in lift coefficients occur (fig. 19(b)). Bump data appear to give a slightly more rearward aerodynamic-center location (fig. 22(a)), although estimated theoretical values of aerodynamic center overlap both sets of wing-alone data. The theoretical aerodynamic-center locations were approximated by applying a correction factor for the effect of chordwise loading, as estimated from reference 14, to the values as determined from reference 13.

The variation of $\partial C_m/\partial C_L$ with Mach number is in good agreement for both the wing-alone and the wing-fuselage configurations. It is of interest that both test methods indicated about the same change in aerodynamic-center position attributable to the fuselage despite the fact that the fuselage was curved for the bump tests.

Drag.- The drag due to lift (fig. 19(c)) is in good agreement except at the higher values of C_L where the higher angles of attack required for the wall models resulted in greater drag increments.

It was in the drag at zero lift that the effects of the Mach number gradients and curvature have been expected to be most evident (fig. 21). The combined effect of these factors resulted in somewhat higher drags for the bump results for both wing alone and wing-fuselage configurations but the rate of drag rise in the transonic range was only slightly less rapid than that obtained on the wall. The wing-alone wall results are in good agreement with the drag data determined from rocket model tests made by the Langley Pilotless Aircraft Research Division of a wing of zero sweep, taper ratio 1, and aspect ratio 3.7 mounted on a cylindrical fuselage, for which interference effects are small (unpublished).

It will be noted also that the effect of the fuselage on the drag at zero lift is essentially the same for the bump and wall tests. The fuselage-alone drag as measured on the wall, is in agreement with the bump fuselage data (fig. 14), except above $M = 1$ where the wall fuselage drag increases more rapidly because of the increased longitudinal velocity gradient at these Mach numbers (fig. 2(b)). In any event, neither the fuselage-alone nor the wing-fuselage drag is very reliable. The wing-fuselage drag indicated for the sting models (fig. 13) is more nearly obtained if the wing-alone drag (fig. 21) is added to the sting or drop-test fuselage drag shown in figure 14.

45° Sweep Configuration

Lift.- The agreement in lift characteristics for the wing-alone data for the bump and wall model is very good both with respect to lift-curve slope (fig. 22(b)) and the lift behavior at the higher angles of attack (fig. 20(a)), although both sets of data give somewhat greater values of lift-curve slope than would be determined from theory (reference 13). The results for the wing-fuselage combination also show excellent agreement as regards lift-curve slope (fig. 22(b)) although in this case differences in lift behavior are evident at the higher angles of attack, perhaps indicating that wing-fuselage interference effects are critical.

Pitching moment.- The pitching-moment behavior for both wing-alone and wing-fuselage configurations is generally in very good agreement as regards the character of variation of C_m with C_L, particularly at the higher values of C_L (fig. 20(b)); however, the bump results do indicate a more rearward aerodynamic-center position (fig. 22(b)) of almost a constant amount throughout the Mach number range as compared with either wall data or theory. As for the $\Lambda = 0^{\circ}$ wing, the theoretical values have been approximated by applying chordwise correction factors estimated from reference 14 to the aerodynamic-center positions determined from reference 13.

The fact that the difference in aerodynamic-center location is almost a constant value at all Mach numbers points to the possibility of an error in positioning of the models relative to the axes of moments. It would take, however, a relative error of about 0.10 inch to account for this difference and the models are believed to be located correctly to within at least 0.01 inch. Some of the differences, therefore, might be attributed to the effect of Mach number gradients. The effect of fuselage curvature would not appear to be so important in this case inasmuch as the same result was obtained for the wing-alone tests.

Drag.- The drag due to lift agrees well in the low lift range but differences are evident at the higher value of C_L (fig. 20(c)). However, it is especially difficult to measure accurate values of drag at the higher values of C_L because of flow unsteadiness. Therefore, some of the drag differences shown may well be within experimental accuracy.

The drag at zero lift for the 45° configuration (fig. 21) shows similar trends to those observed for the 0° configuration and the notable effect of sweepback in diminishing the rate of drag rise is reflected in both sets of data. The drag determined for the wall tests is slightly lower at the lower Mach numbers but the rate of drag rise for the 45° configuration is in excellent agreement for both models, indicating little effect of Mach number gradient or curvature. The agreement between the wing-alone results and the rocket data is noteworthy,

particularly in view of the differences in Reynolds number. The rocket drag data used in this comparison are unpublished and differ from those presented in reference 8 (and used in fig. 15), in that a fuselage having a cylindrical section at the wing root was used instead of the fuselage described by table I.

Comparison with Sting Data

A comparison at several subsonic Mach numbers of the bump, wall, and 8-foot sting data is presented in figure 23 for the 0° and 45° wing-fuselage configurations.

For the 0° configuration, the lift characteristics, particularly at high angles of attack, are somewhat different for all three methods. For the 45° configuration, however, the agreement in lift between 8-foot sting results and wall results is very good. The pitching-moment characteristics exhibited by the wall model appear to agree with the 8-foot sting results for the 45° configuration, particularly as regards (1) the lift coefficient at which the moment curve breaks unstable and (2) the aerodynamic-center position and its change with Mach number. The wall data for the 0° configuration, on the other hand, are in no better agreement with the 8-foot sting results than the bump data.

The drag due to lift does not show any extreme differences (fig. 23(c)) and, as far as the drag at zero lift is concerned, neither the bump nor wall data for wing-fuselage drag can be considered reliable because of the extremely high drag obtained with the fuselage alone (fig. 14).

CONCLUSIONS

Based on a study of the aerodynamic characteristics of a family of four wing-fuselage configurations of 0°, 35°, 45°, and 60° sweepback as determined from bump model tests, sting-supported wind-tunnel model tests, and a few rocket model tests, the following conclusions are indicated:

1. Qualitatively, the bump model results and the sting model results indicated about the same relative effects of sweepback and Mach number on the aerodynamic characteristics of the wing-fuselage family except for drag at zero lift. Quantitatively, significant differences in results were evident. In general, wherever sudden changes in lift, drag, and pitching moment occurred, the bump model results indicated less rapid changes with Mach number and angle of attack than the sting model results.

2. Lift-curve slopes as determined from bump model tests were generally a little higher, and the variation with Mach number somewhat less pronounced, than were obtained from sting-model tests.

3. Drag due to lift was generally in fair agreement for the bump and sting models, but discrepancies were evident whenever differences occurred in the angle of attack required to support the same lift.

4. Drag at zero lift as determined by bump tests for either the fuselage alone or for the wing-fuselage combinations, is considered to be unreliable because of exhibited discrepancies with the results of sting model tests and rocket model tests, particularly at Mach numbers above 1. However, wing-alone drag as determined from bump models appeared to agree well with available rocket model data throughout the transonic range.

5. Aerodynamic-center position as determined from bump data was generally more rearward than was found from sting model results, particularly for the 60° sweep configuration.

6. A study of the effect of Mach number gradient and bump curvature on the bump results indicated that the principal effect of these factors on the wings investigated was to move the aerodynamic-center position somewhat more rearward. No consistent effect of these variables was noticed on other aerodynamic parameters.

7. It was important in comparing the results obtained in the different test facilities to consider the relative flexibility of the model installations because the aeroelastic effects exhibited were sufficiently different in some cases to affect the comparison, particularly in regard to aerodynamic-center position.

Langley Aeronautical Laboratory
National Advisory Committee for Aeronautics
Langley Air Force Base, Va.

REFERENCES

1. Goodson, Kenneth W., and Morrison, William D., Jr.: Aerodynamic Characteristics of a Wing with Unswept Quarter-Chord Line, Aspect Ratio 4, Taper Ratio 0.6, and NACA 65A006 Airfoil Section. Transonic-Bump Method. NACA RM L9H22, 1949.

2. Sleeman, William C., Jr., and Becht, Robert E.: Aerodynamic Characteristics of a Wing with Quarter-Chord Line Swept Back 35°, Aspect Ratio 4, Taper Ratio 0.6, and NACA 65A006 Airfoil Section. Transonic-Bump Method. NACA RM L9B25, 1949.

3. Weil, Joseph, and Goodson, Kenneth W.: Aerodynamic Characteristics of a Wing with Quarter-Chord Line Swept Back 45°, Aspect Ratio 4, Taper Ratio 0.6, and NACA 65A006 Airfoil Section. Transonic-Bump Method. NACA RM L9A21, 1949.

4. King, Thomas J., Jr., and Myers, Boyd C., II: Aerodynamic Characteristics of a Wing with Quarter-Chord Line Swept Back 60°, Aspect Ratio 4, Taper Ratio 0.6, and NACA 65A006 Airfoil Section. Transonic-Bump Method. NACA RM L9G27, 1949.

5. Sleeman, William C., Jr., and Morrison, William D., Jr.: Aerodynamic Characteristics of a Wing with Quarter-Chord Line Swept Back 35°, Aspect Ratio 6, Taper Ratio 0.6, and NACA 65A006 Airfoil Section. Transonic-Bump Method. NACA RM L9K10a, 1949.

6. Goodson, Kenneth W., and Few, Albert G., Jr.: Aerodynamic Characteristics of a Wing with Quarter-Chord Line Swept Back 45°, Aspect Ratio 6, Taper Ratio 0.6, and NACA 65A006 Airfoil Section. Transonic-Bump Method. NACA RM L9I08, 1949.

7. Osborne, Robert S.: A Transonic Wing Investigation in the Langley 8-Foot High-Speed Tunnel at High Subsonic Mach Numbers and at a Mach Number of 1.2. Wing-Fuselage Configuration with a Wing of 45° Sweepback, Aspect Ratio 4, Taper Ratio 0.6, and NACA 65A006 Airfoil Section. NACA RM L50H08, 1950.

8. Katz, Ellis: Flight Investigations from High Subsonic to Supersonic Speeds to Determine the Zero-Lift Drag of a Transonic Research Vehicle Having Wings of 45° Sweepback, Aspect Ratio 4, Taper Ratio 0.6, and NACA 65A006 Airfoil Sections. NACA RM L9H30, 1949.

9. Johnson, Harold I.: Measurements of Aerodynamic Characteristics of a 35° Sweptback NACA 65-009 Airfoil Model with $\frac{1}{4}$-Chord Plain Flap by the NACA Wing-Flow Method. NACA RM L7F13, 1947.

10. Herriot, John G.: Blockage Corrections for Three-Dimensional-Flow Closed-Throat Wind Tunnels, with Consideration of the Effect of Compressibility. NACA RM A7B28, 1947.

11. Thompson, Jim Rogers: Measurements of the Drag and Pressure Distribution on a Body of Revolution throughout Transition from Subsonic to Supersonic Speeds. NACA RM L9J27, 1950.

12. Letko, William, and Wolhart, Walter D.: Effect of Sweepback on the Low-Speed Static and Rolling Stability Derivatives of Thin Tapered Wings of Aspect Ratio 4. NACA RM L9F14, 1949.

13. DeYoung, John: Theoretical Additional Span Loading Characteristics of Wings with Arbitrary Sweep, Aspect Ratio, and Taper Ratio. NACA TN 1491, 1947.

14. Falkner, V. M.: Calculated Loadings Due to Incidence of a Number of Straight and Swept-Back Wings. Rep. No. 11, 542, British A.R.C., June 5, 1948.

TABLE I.- TRANSONIC FUSELAGE ORDINATES

[Basic fineness ratio 12; actual fineness ratio 10 achieved by cutting off the rear one-sixth of the body]

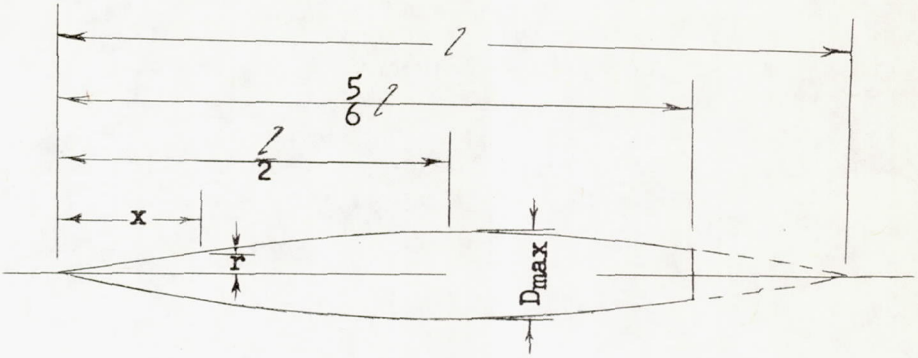

Ordinates			
x/l	r/l	x/l	r/l
0	0	0	0
.005	.00231	.4500	.04143
.0075	.00298	.5000	.04167
.0125	.00428	.5500	.04130
.0250	.00722	.6000	.04024
.0500	.01205	.6500	.03842
.0750	.01613	.7000	.03562
.1000	.01971	.7500	.03128
.1500	.02593	.8000	.02526
.2000	.03090	.8338	.02000
.2500	.03465	.8500	.01852
.3000	.03741	.9000	.01125
.3500	.03933	.9500	.00439
.4000	.04063	1.0000	0
L. E. radius = 0.0005l			

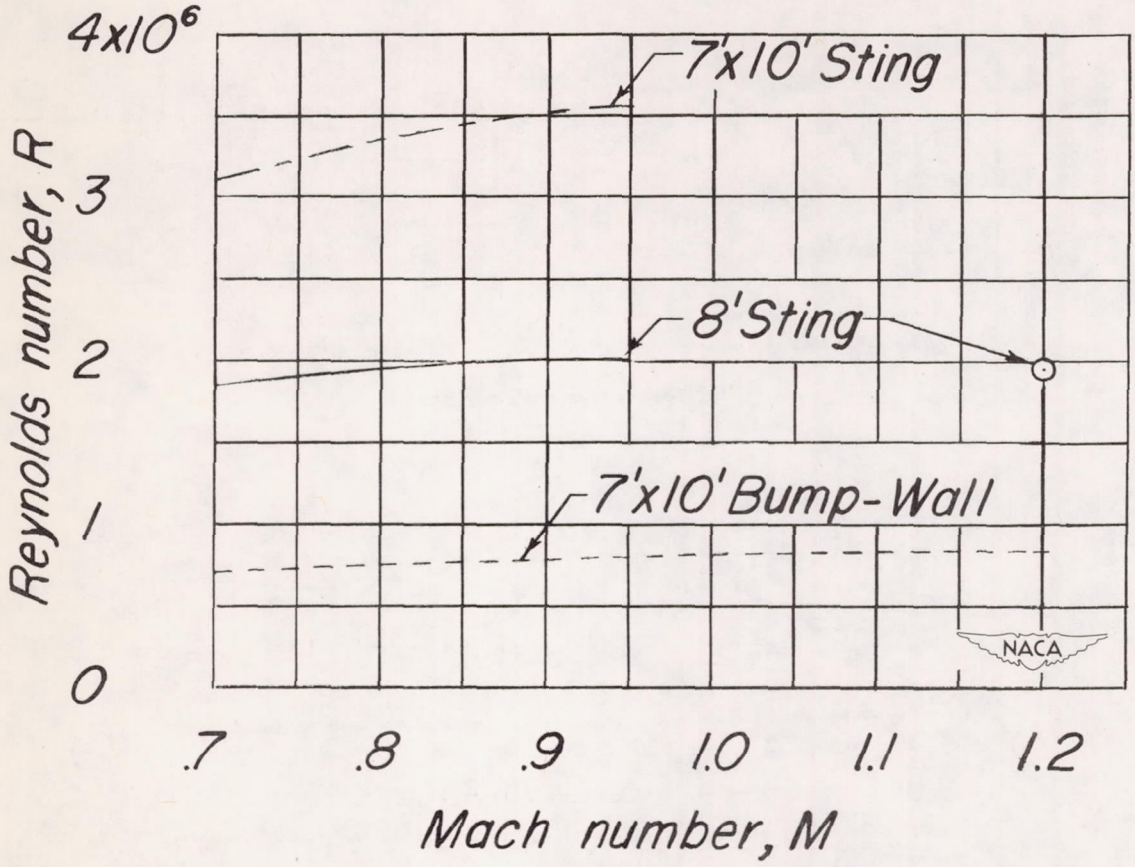

Figure 1.- Variation of Reynolds number with Mach number for various test techniques.

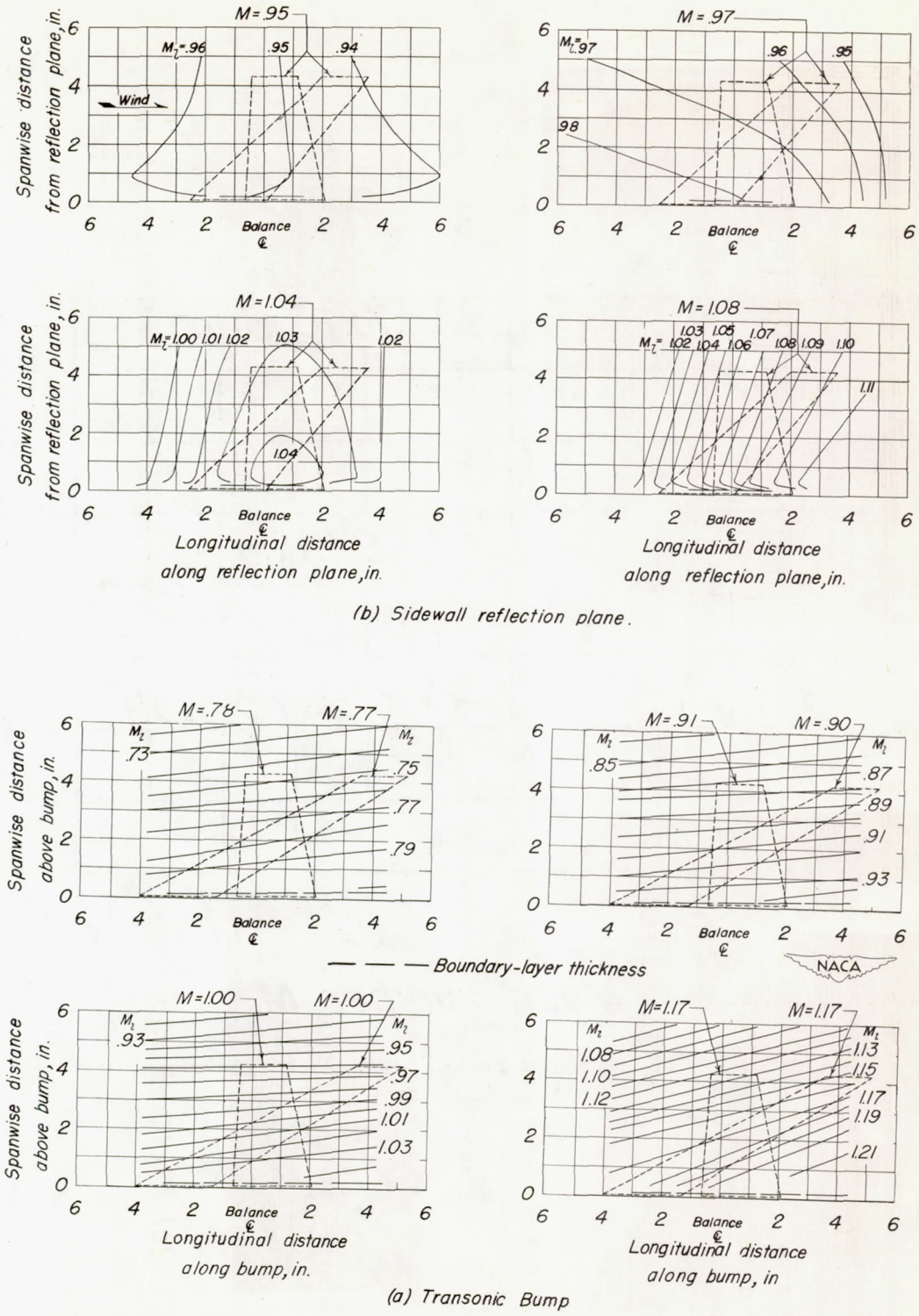

Figure 2.- Typical Mach number contours in the region of the model location for two transonic test techniques used in the Langley high-speed 7- by 10-foot tunnel.

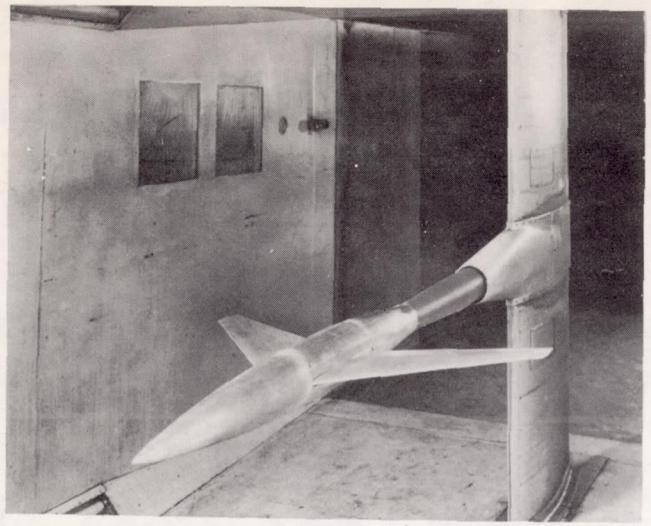

(a) 7'x10' Sting.

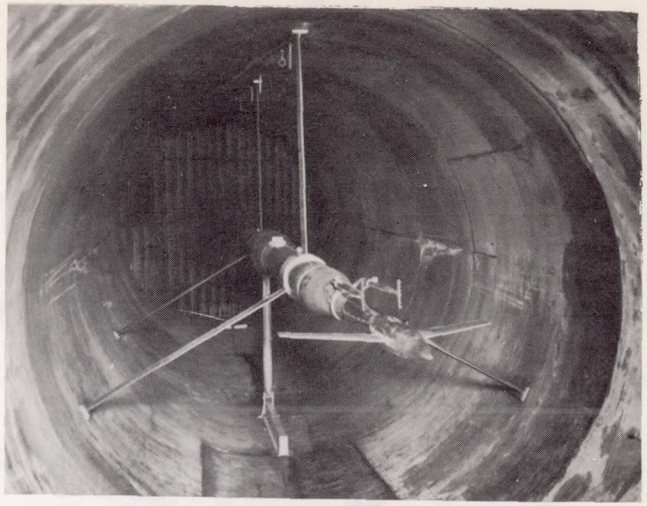

(b) 8' Sting.

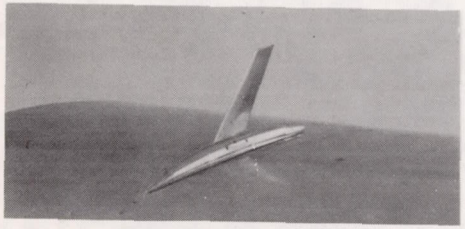

(c) 7'x10' Bump.

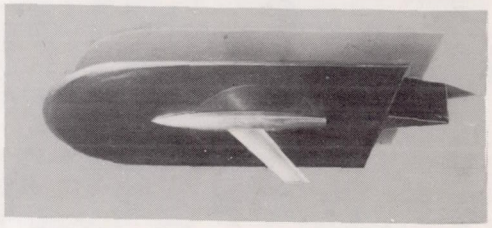

(d) 7'x 10' Wall reflection plane.

NACA
L-64928

Figure 3.- Photographs of a wing-fuselage model mounted in four different test facilities.

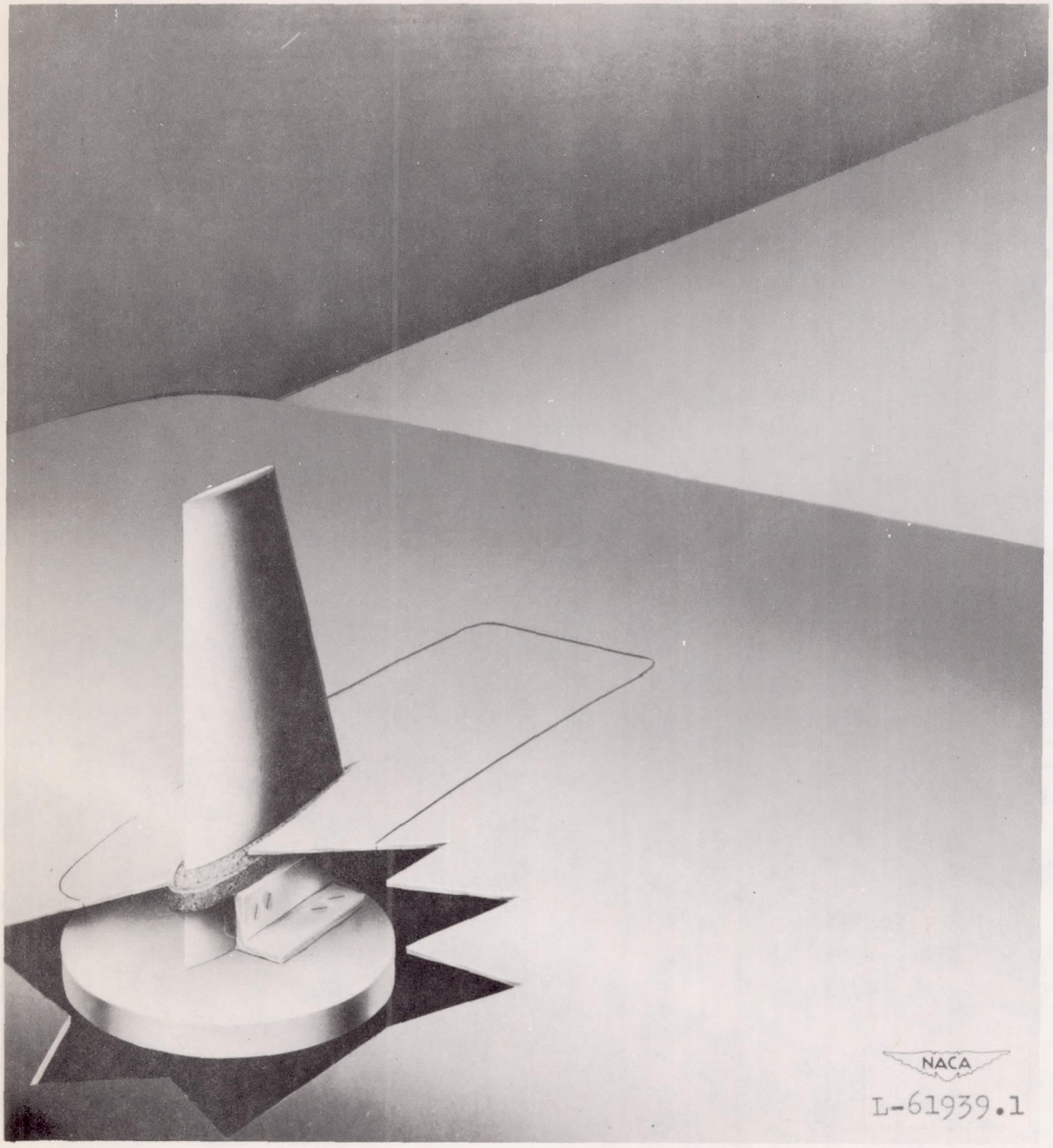

Figure 4.- A view of a wing model mounted on the transonic bump showing the foam-rubber wiper seal.

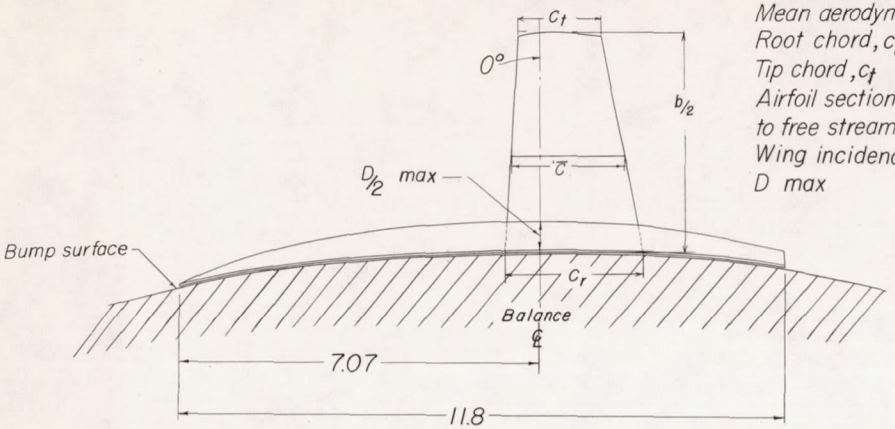

Aspect ratio	4.0
Taper ratio	0.6
Wing area	0.125 sq ft
Wing span	8.486 in.
Mean aerodynamic chord	2.166 in.
Root chord, c_r	2.652 in.
Tip chord, c_t	1.591 in.
Airfoil section parallel to free stream.	NACA 65A006
Wing incidence	0°
D max	1.18 in.

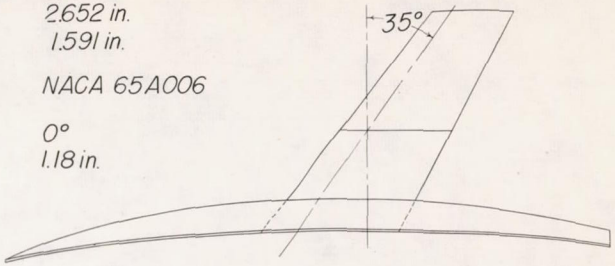

Note:
Same model wings with unbent fuselages used in wall reflection plane technique.

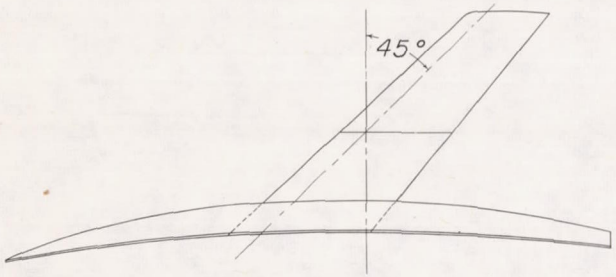

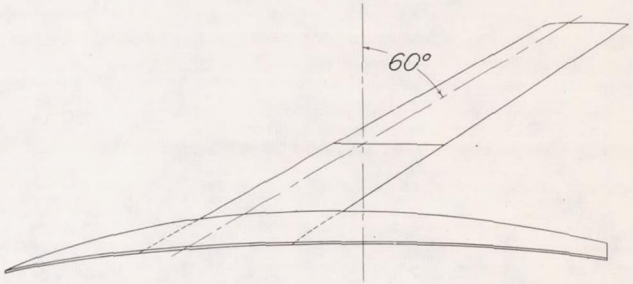

7'x10' BUMP MODELS

NACA

0 1 2
Scale, inches

Figure 5.- Drawing of the wing-fuselage configurations used on the transonic bump.

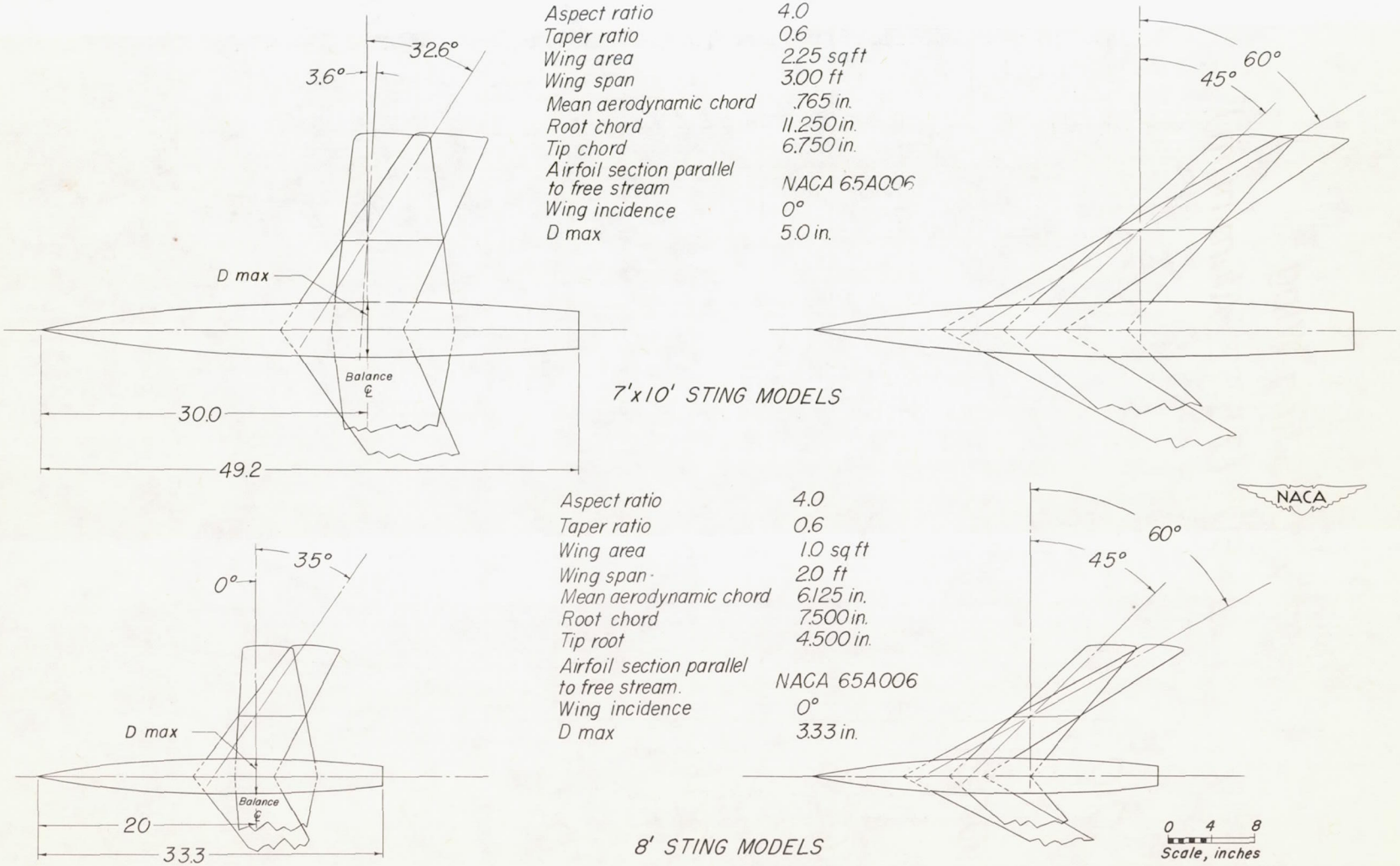

Figure 6.- Drawing of sting models used in two different test facilities.

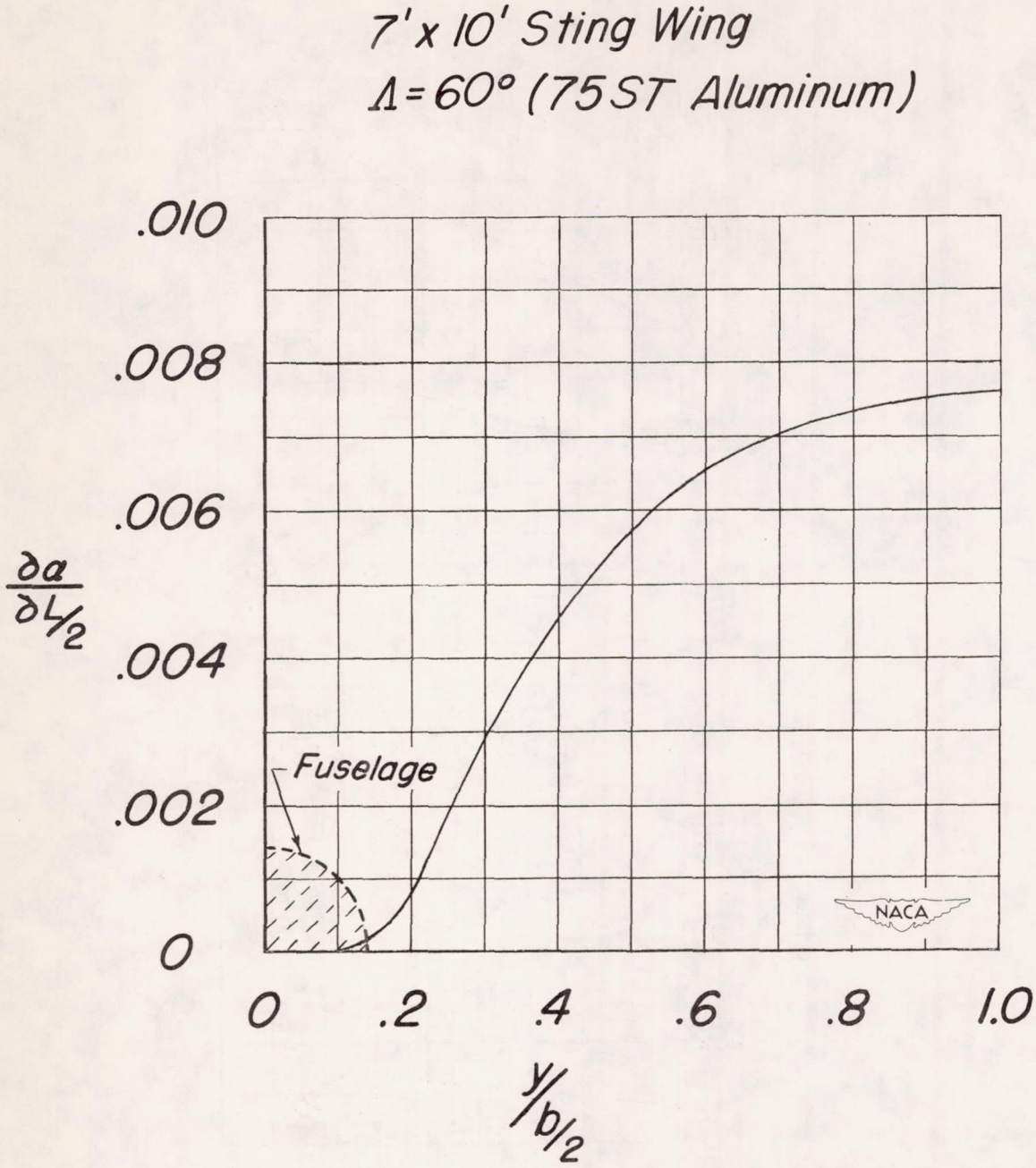

Figure 7.- Measured twist per unit of panel lift, degrees per pound, along the span of a 60° sweptback wing model.

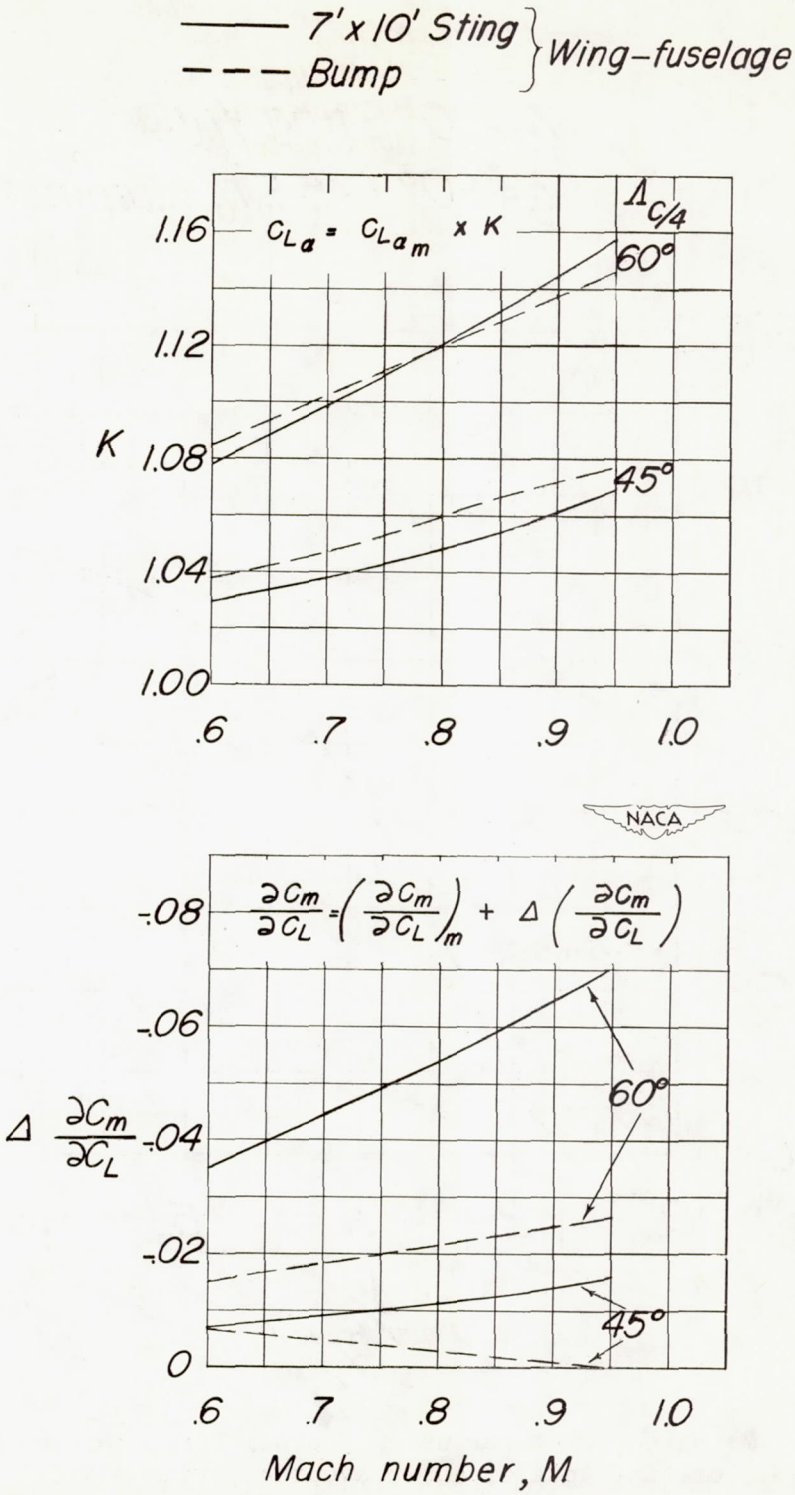

Figure 8.- Correction factors used to determine aerodynamic effects as a result of twist for two different models in two test facilities.

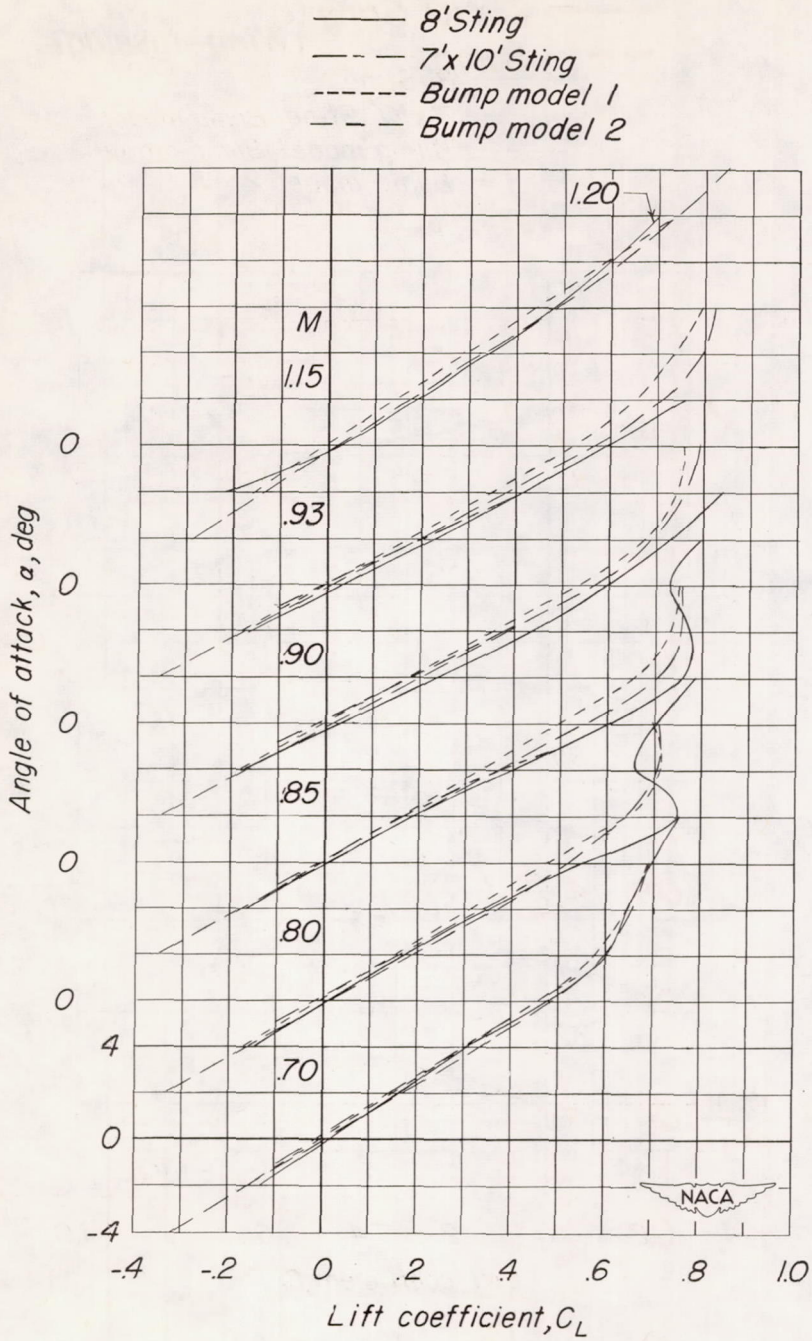

(a) α against C_L.

Figure 9.- Wing-fuselage aerodynamic characteristics as determined from different test facilities for a model with unswept wing, aspect ratio 4, taper ratio 0.6, and NACA 65A006 airfoil section parallel to free stream.

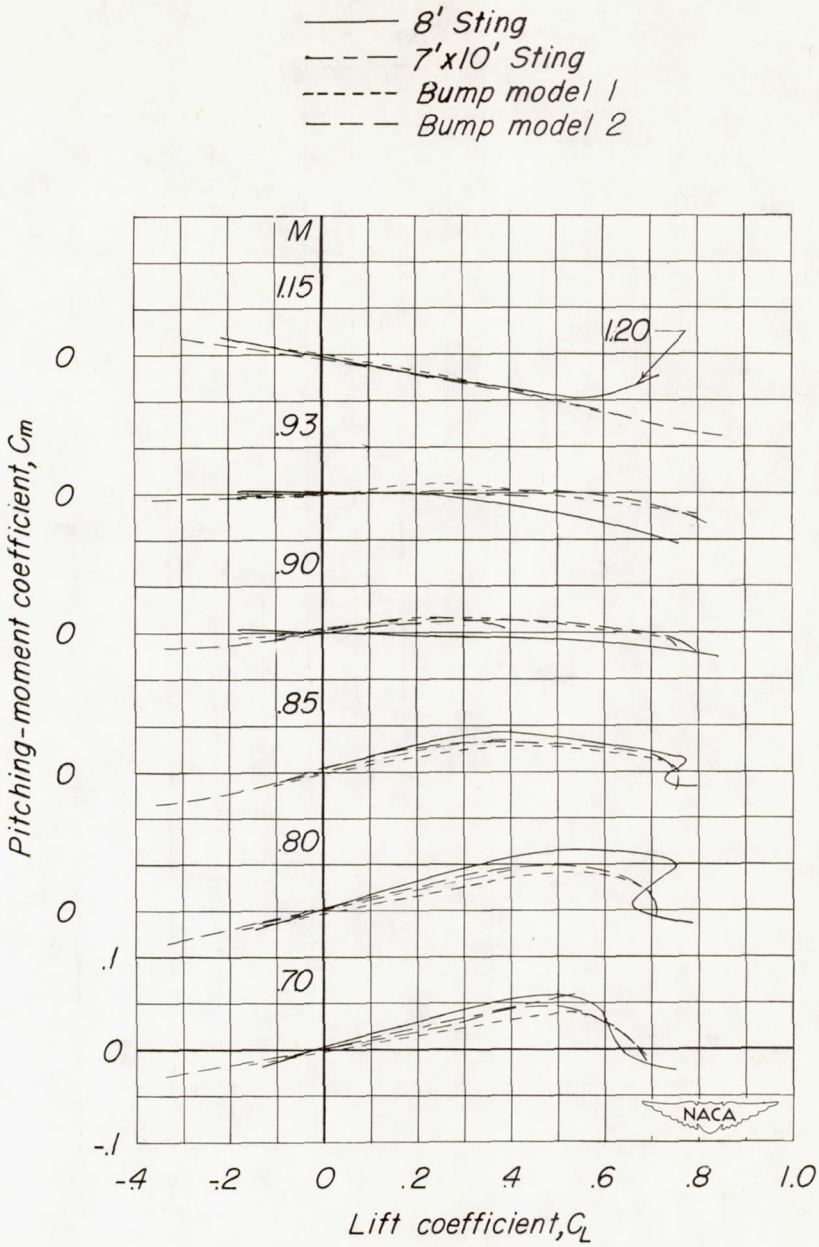

(b) C_m against C_L.

Figure 9.- Continued.

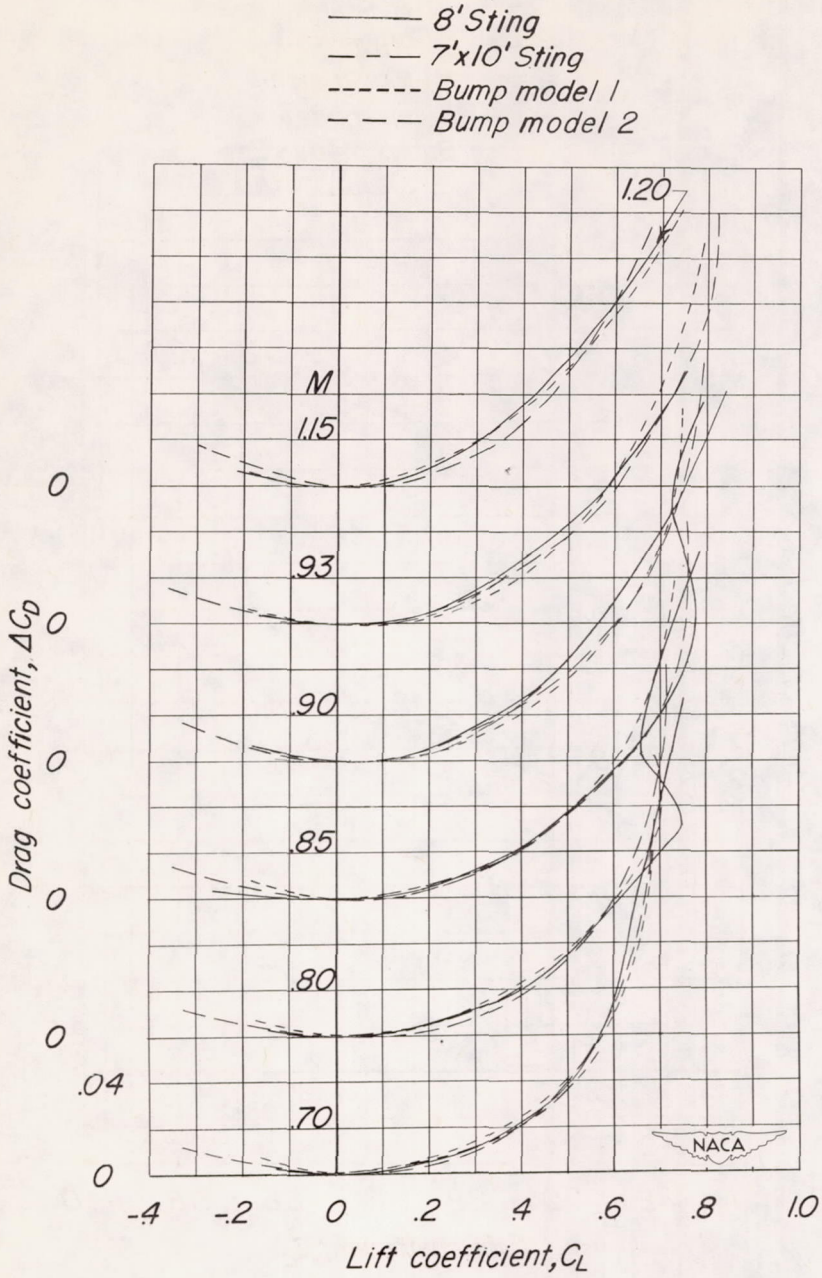

(c) ΔC_D against C_L.

Figure 9.- Concluded.

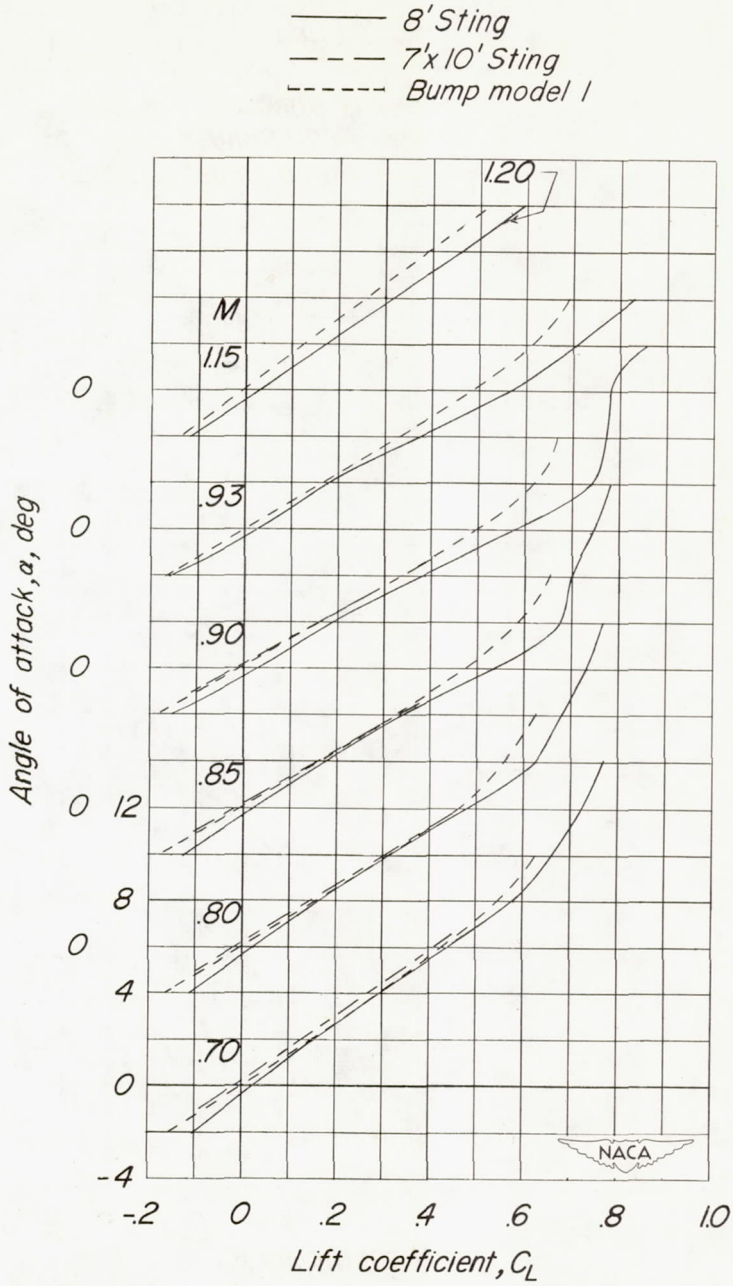

(a) α against C_L.

Figure 10.- Wing-fuselage aerodynamic characteristics as determined from different test facilities for a model with 35° sweptback wing, aspect ratio 4, taper ratio 0.6, and NACA 65A006 airfoil section parallel to free stream.

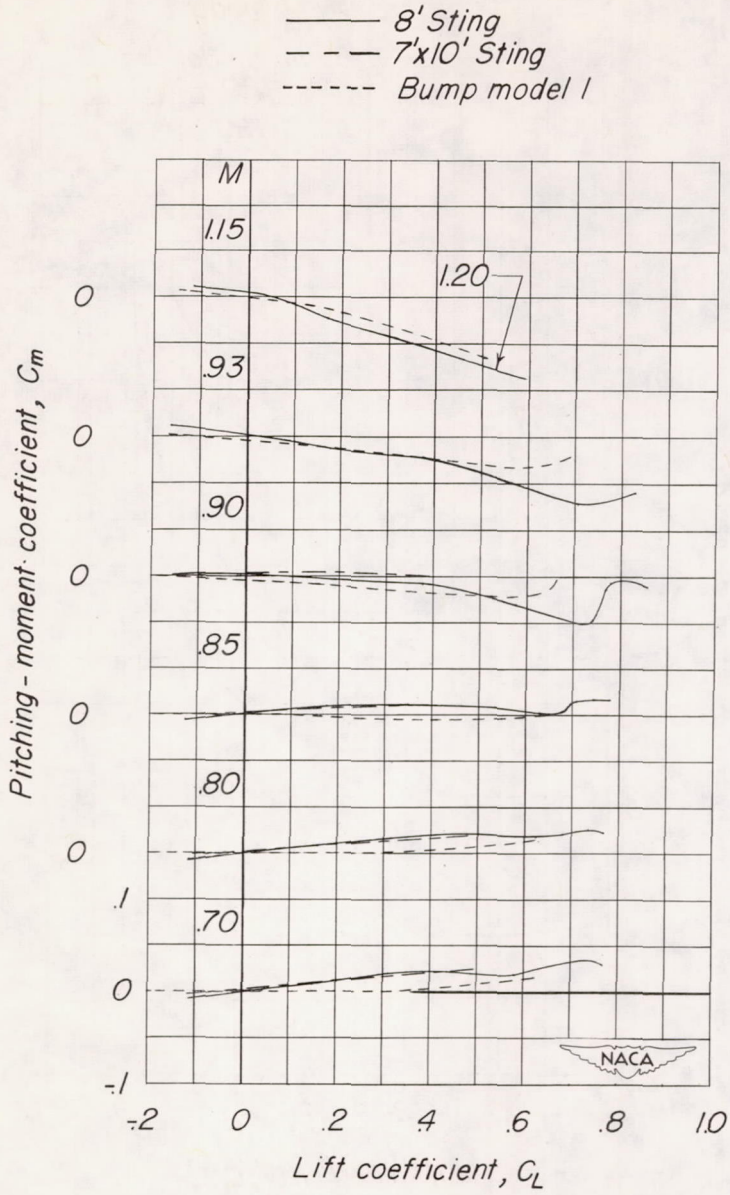

(b) C_m against C_L.

Figure 10.- Continued.

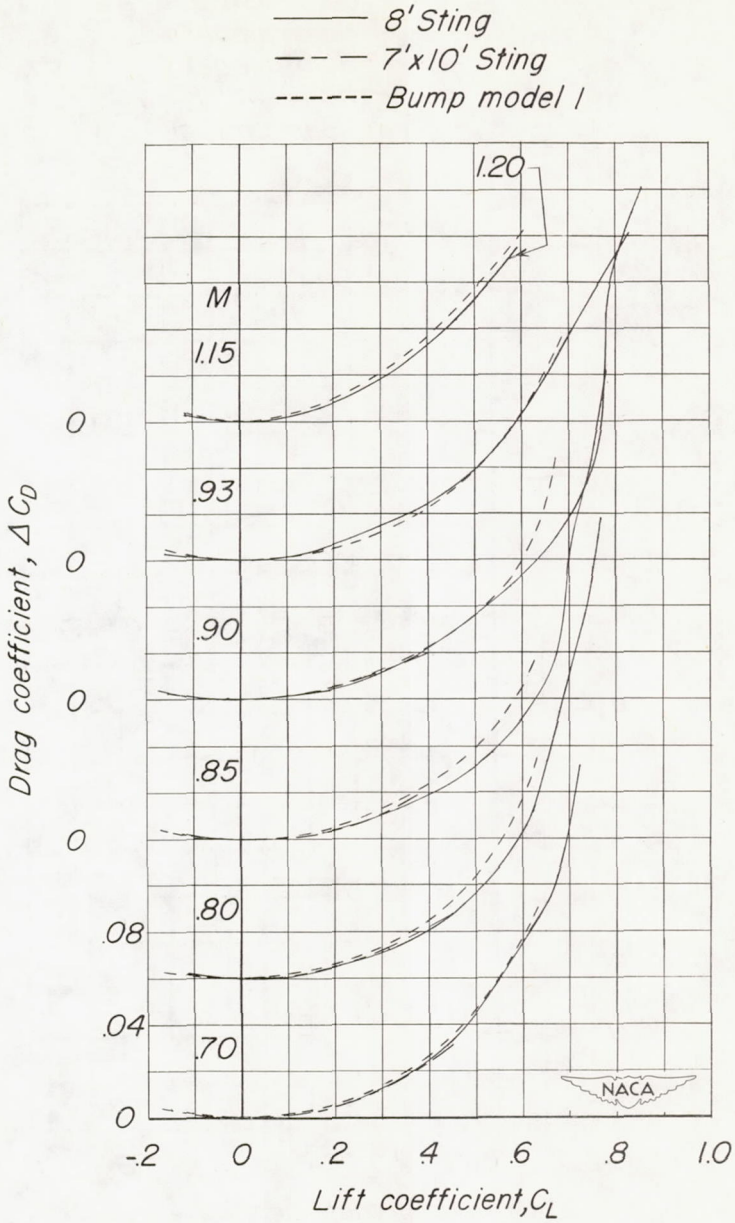

(c) ΔC_D against C_L.

Figure 10.- Concluded.

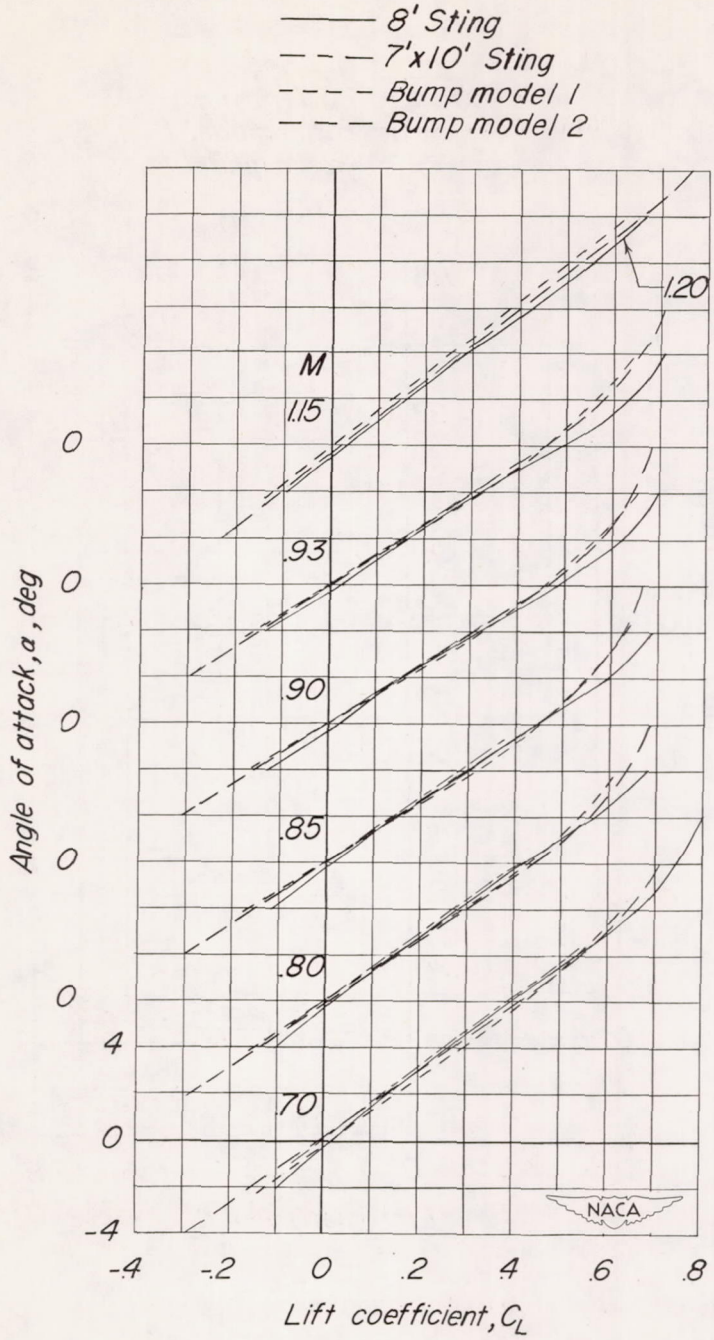

(a) α against C_L.

Figure 11.- Wing-fuselage aerodynamic characteristics as determined from different test facilities for a model with 45° sweptback wing, aspect ratio 4, taper ratio 0.6, and NACA 65A006 airfoil section parallel to free stream.

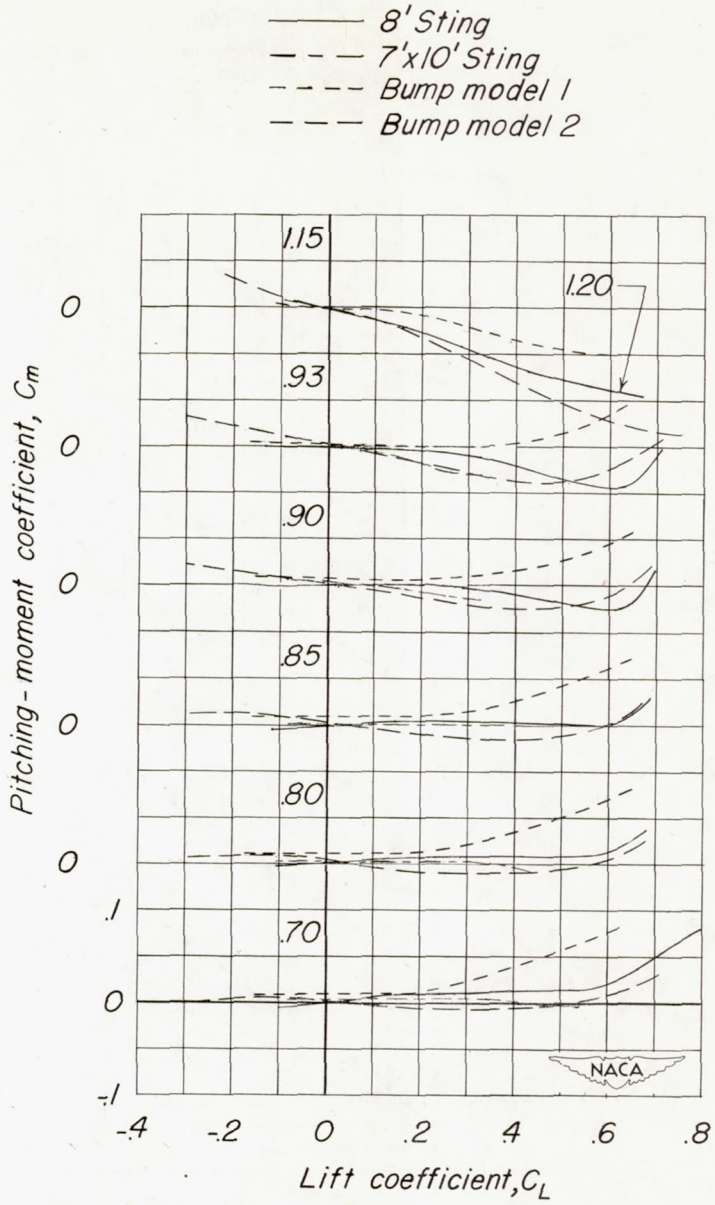

(b) C_m against C_L.

Figure 11.- Continued.

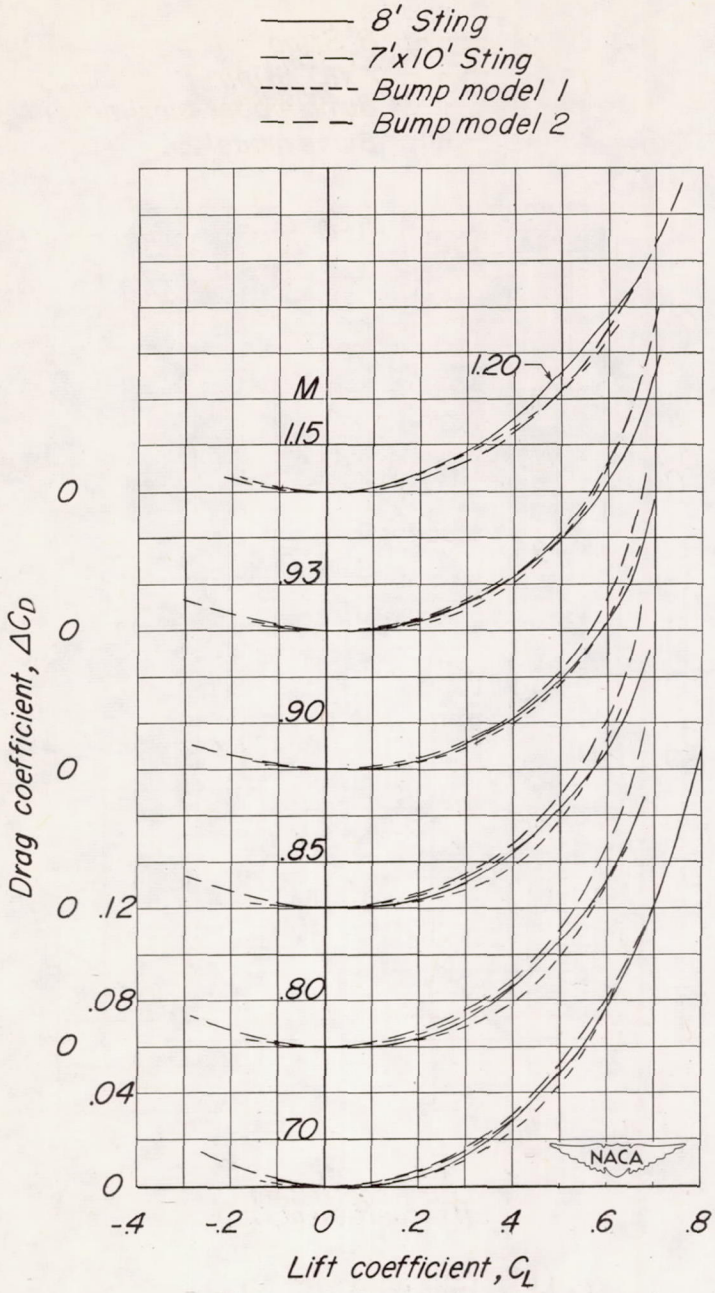

(c) ΔC_D against C_L.

Figure 11.- Concluded.

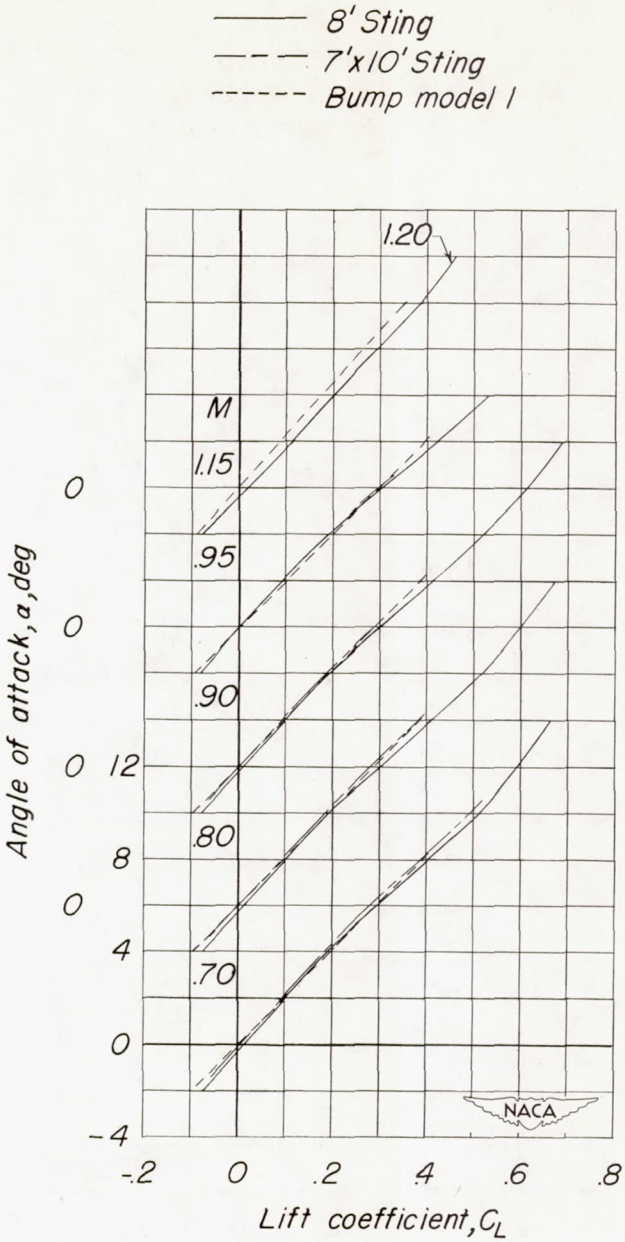

(a) α against C_L.

Figure 12.- Wing-fuselage aerodynamic characteristics as determined from different test facilities for a model with 60° sweptback wing, aspect ratio 4, taper ratio 0.6, and NACA 65A006 airfoil section parallel to free stream.

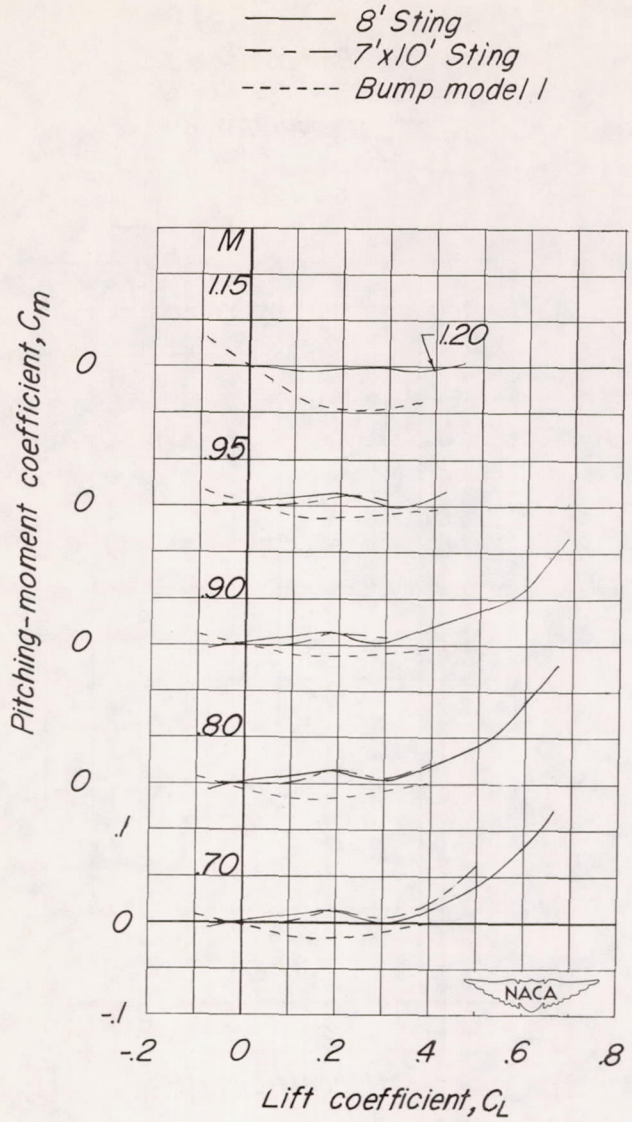

(b) C_m against C_L.

Figure 12.- Continued.

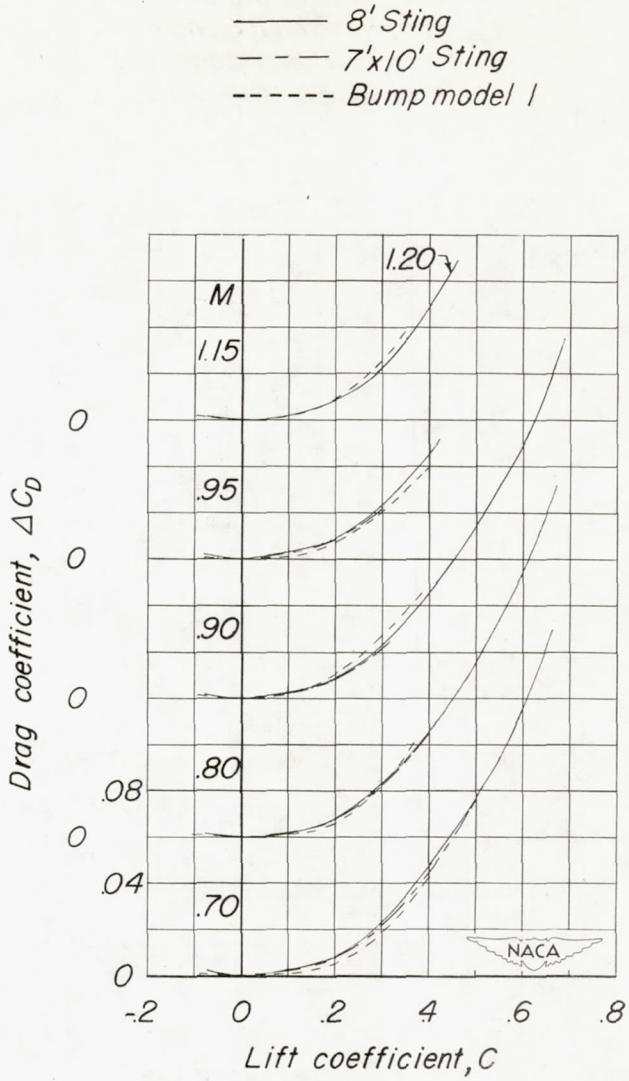

(c) ΔC_D against C_L.

Figure 12.- Concluded.

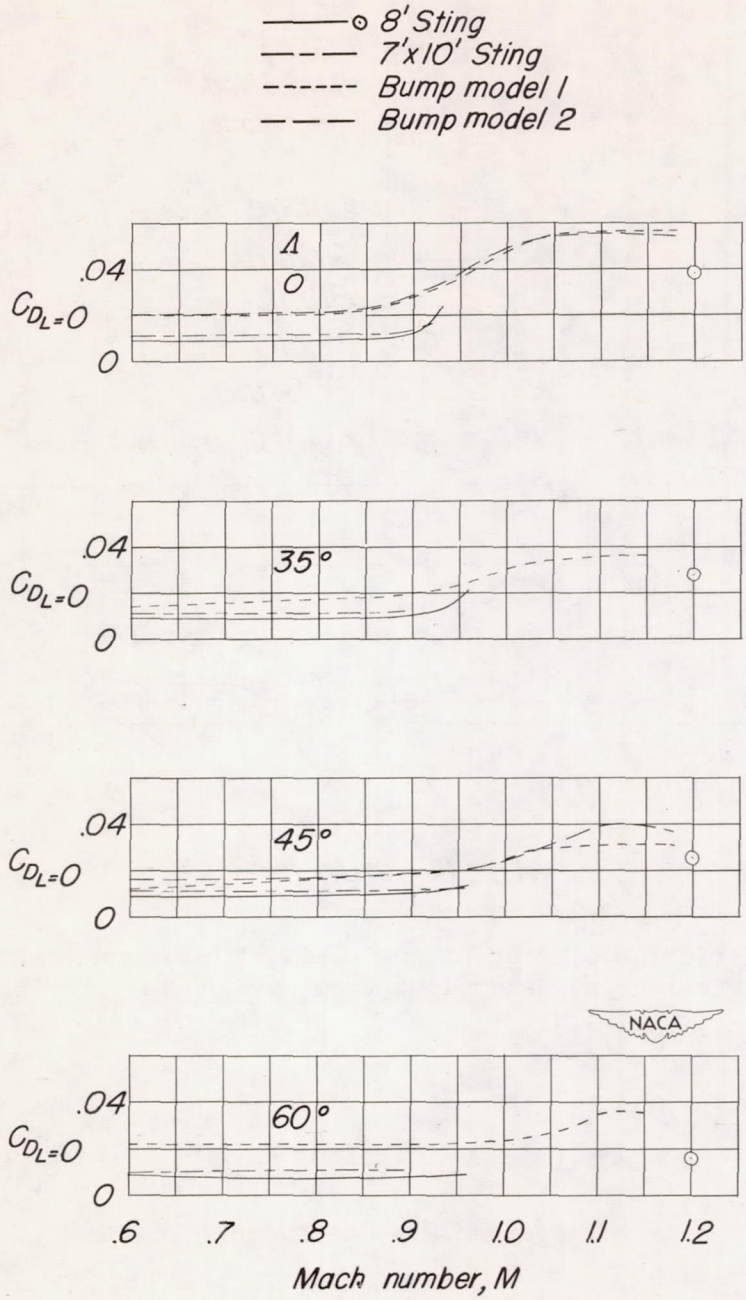

Figure 13.- Effect of sweep and Mach number on drag at zero lift for a wing-fuselage configuration in different test facilities.

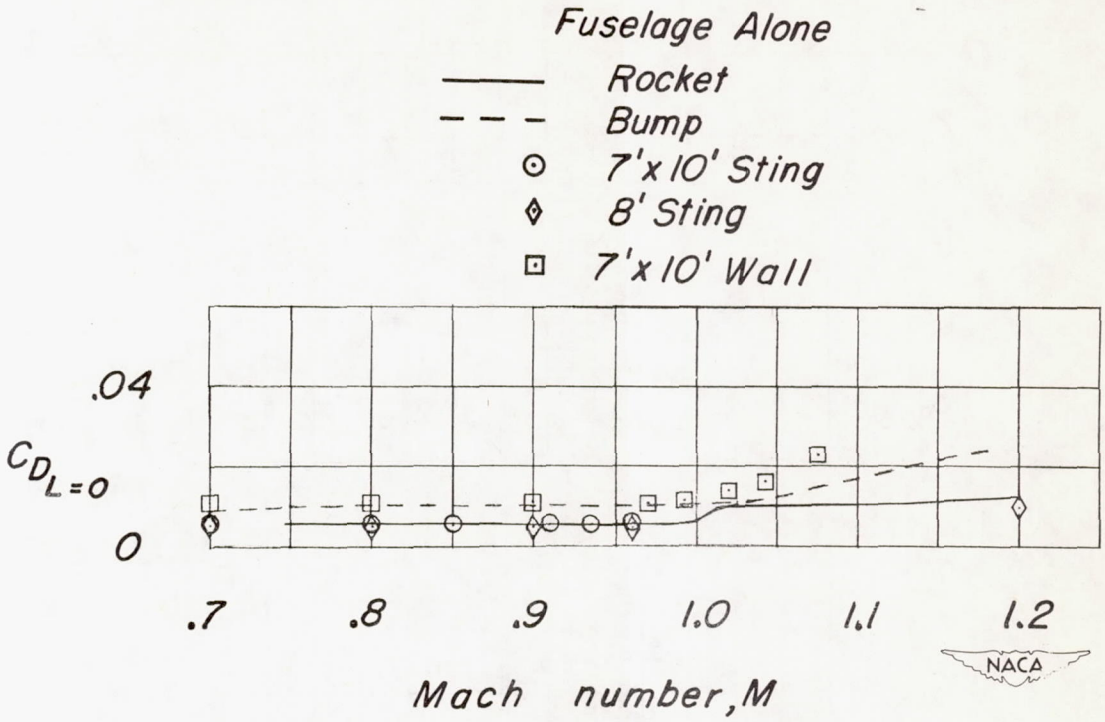

Figure 14.- Variation of drag at zero lift with Mach number for the transonic fuselage as determined from several test facilities.

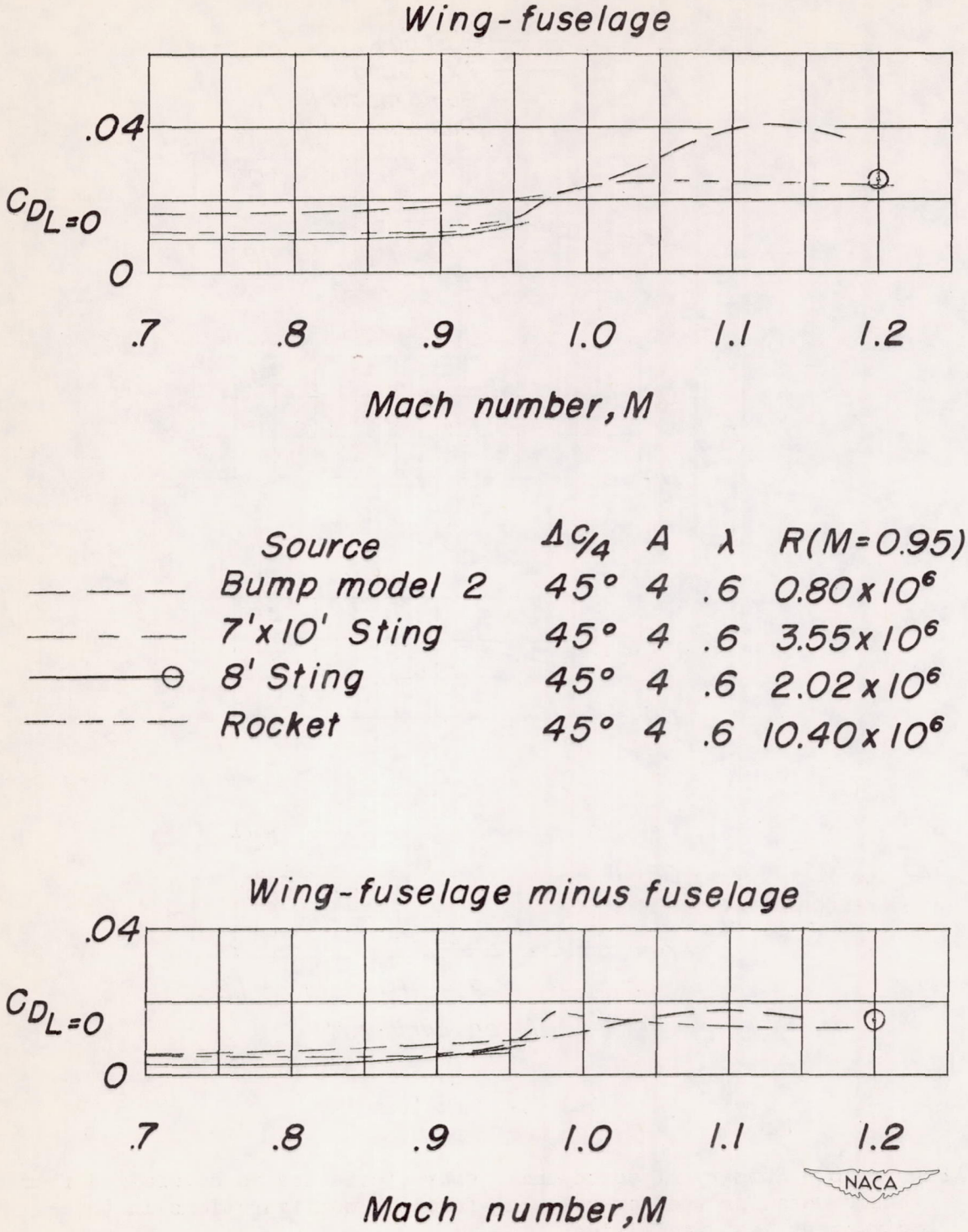

Figure 15.- A comparison of drag at zero lift for two configurations as determined from three different test techniques.

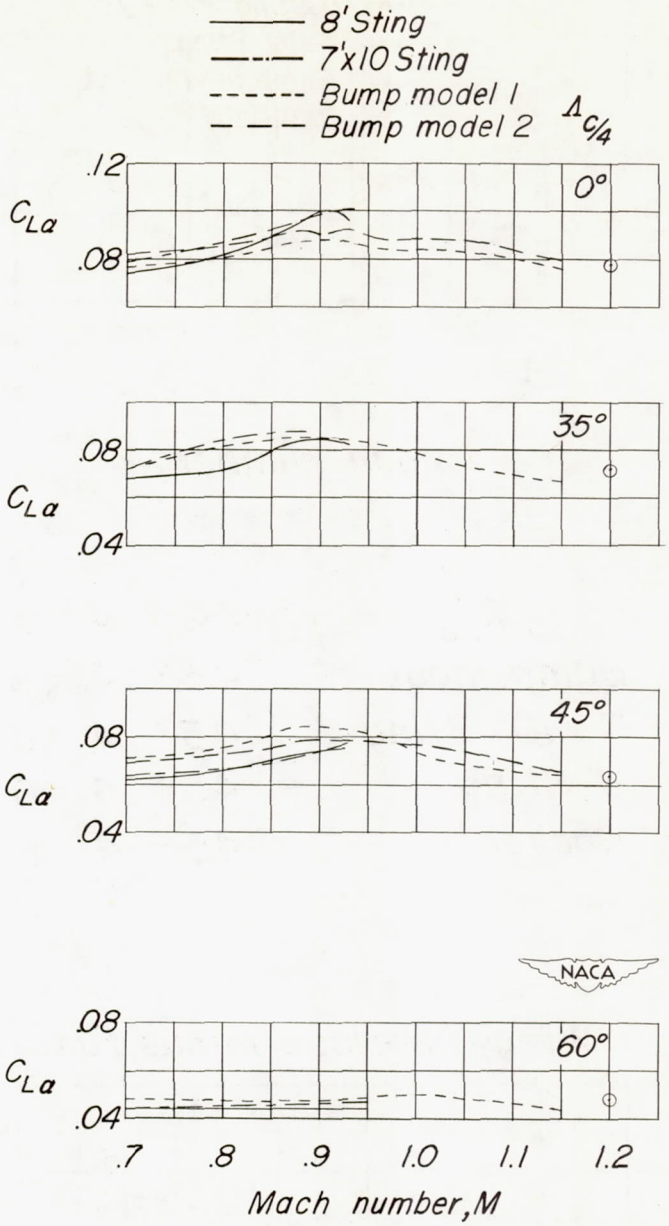

(a) C_{L_α} against M.

Figure 16.- Summary of aerodynamic characteristics as determined from basic data for the several wing-fuselage configurations in three different test facilities.

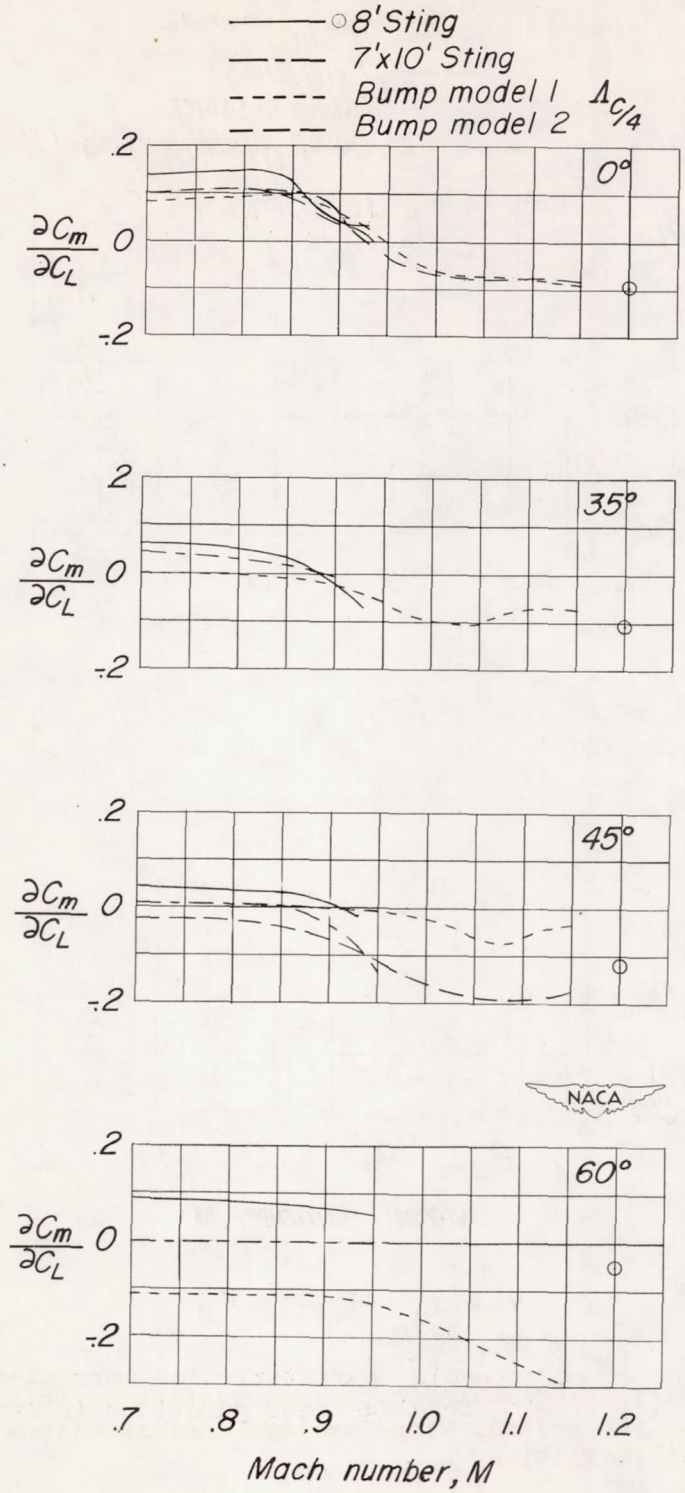

(b) C_m/C_L against M.

Figure 16.- Concluded.

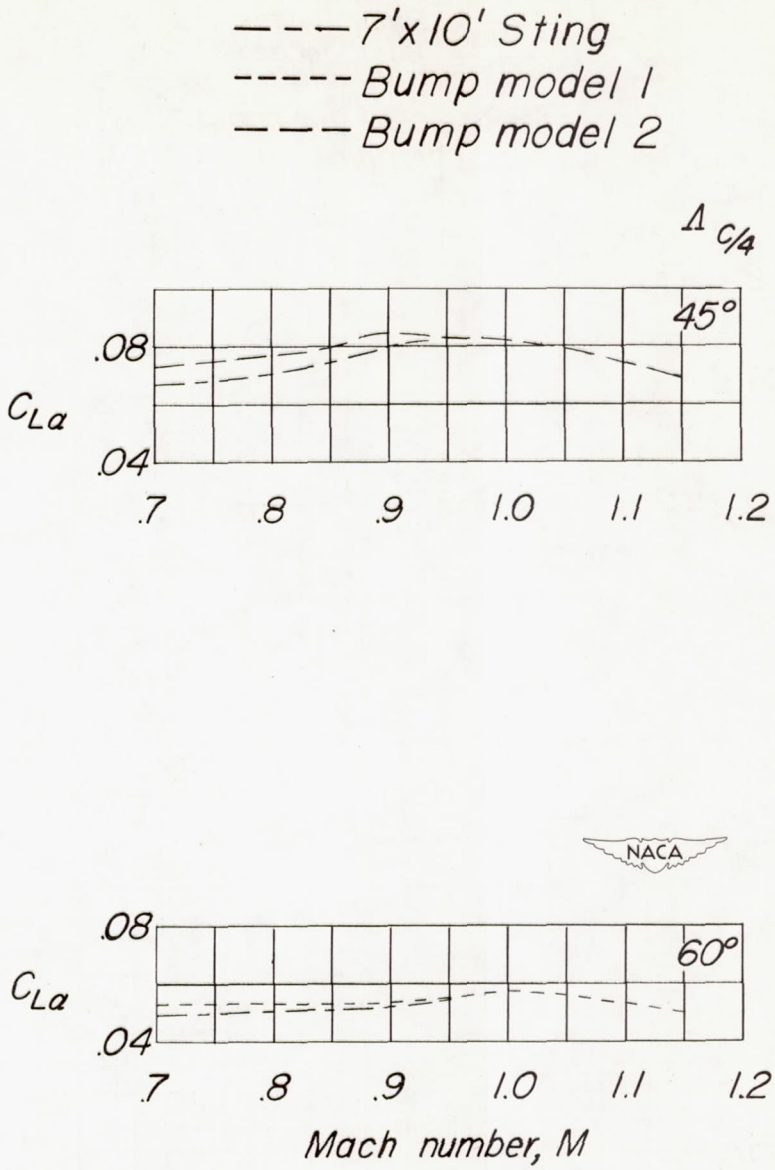

(a) C_{L_α} against M.

Figure 17.- Summary of aerodynamic characteristics corrected for aerodynamic twist for two wing-fuselage configurations in two different test facilities.

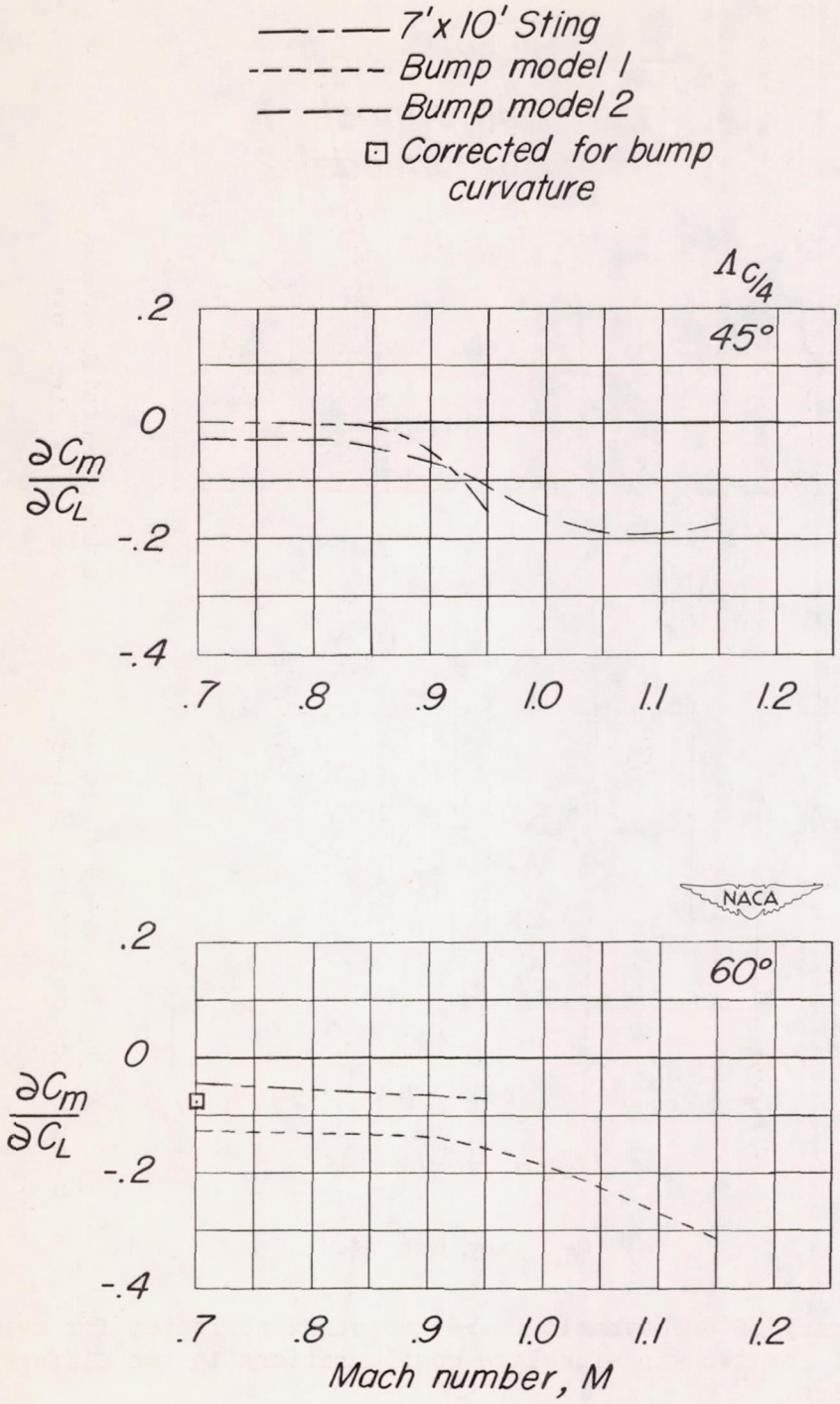

(b) $\partial C_m/C_L$ against M.

Figure 17.- Concluded.

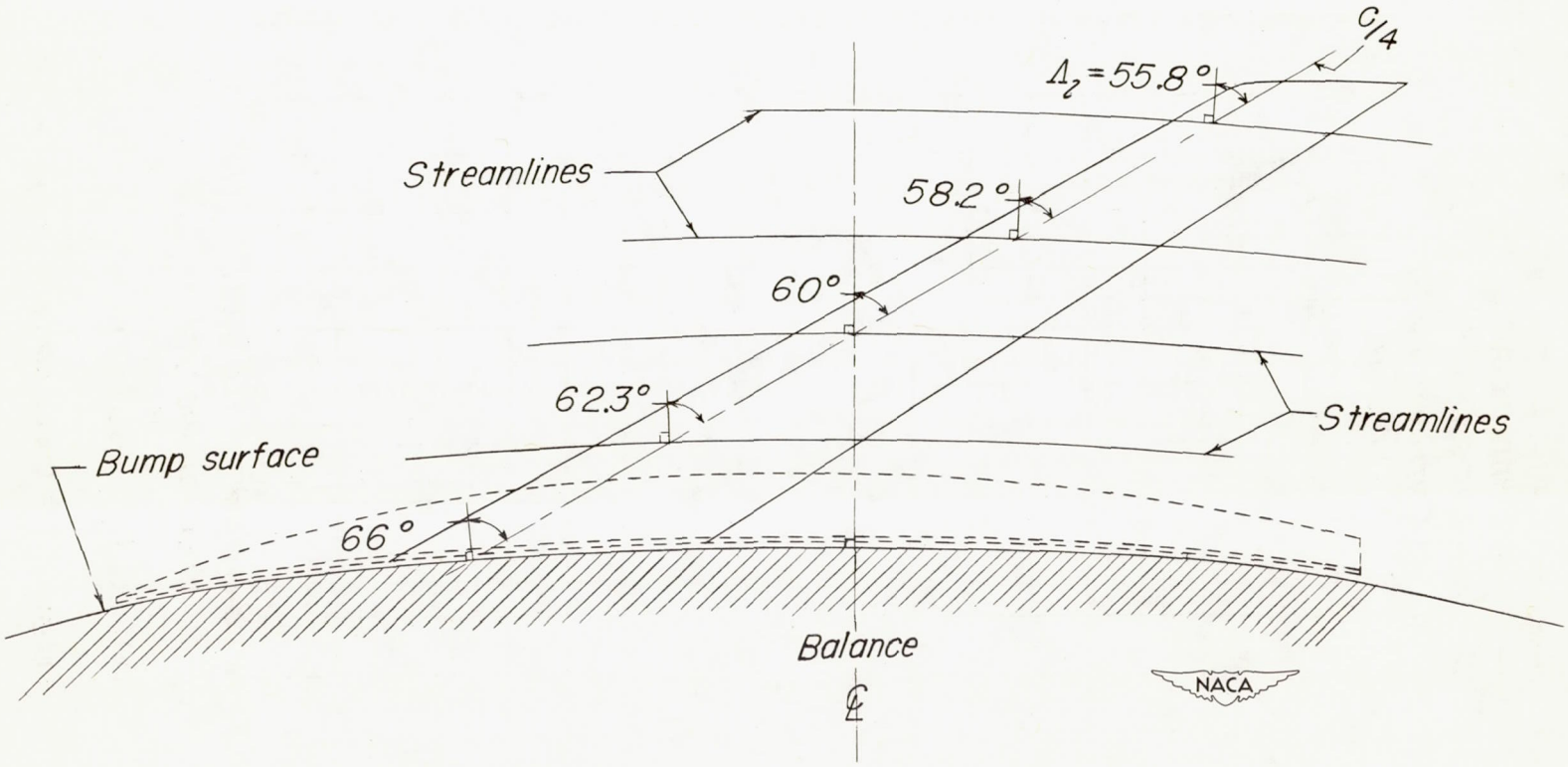

Figure 18.- The effective sweep angle at several spanwise stations on a 60° sweptback wing model when placed in the curved flow field over the bump.

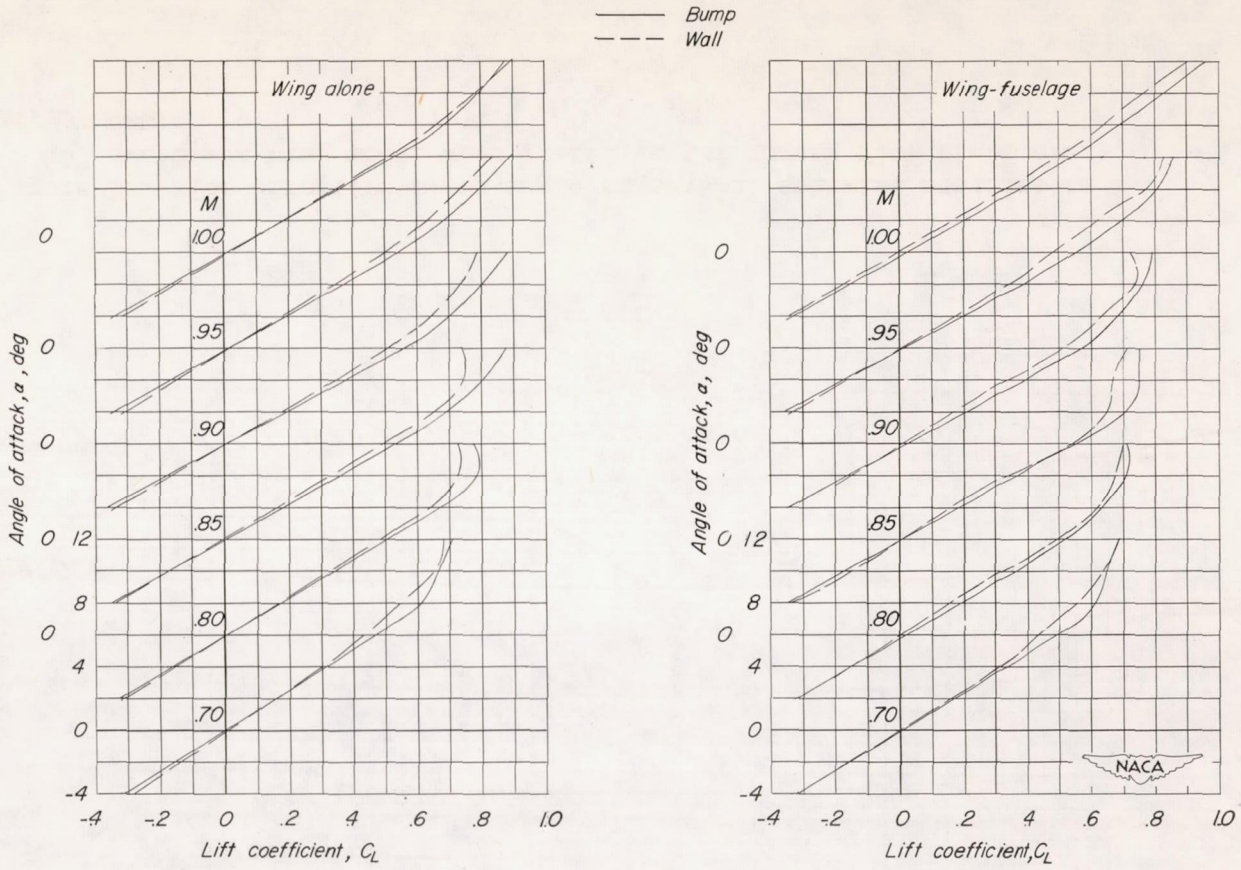

(a) α against C_L.

Figure 19.- Aerodynamic characteristics of wing-alone and wing-fuselage configurations as determined from two different test techniques for an unswept wing, aspect ratio 4, taper ratio 0.6, and NACA 65A006 airfoil section.

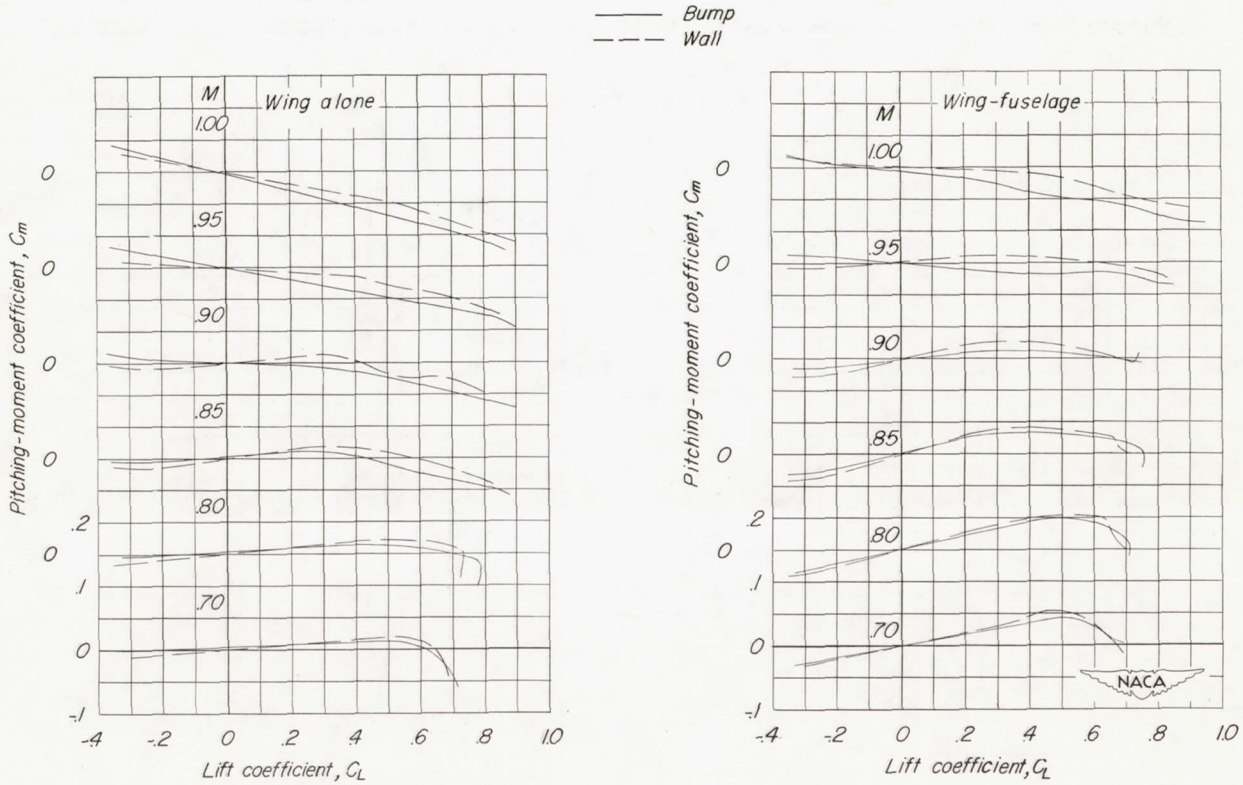

(b) C_m against C_L.

Figure 19.- Continued.

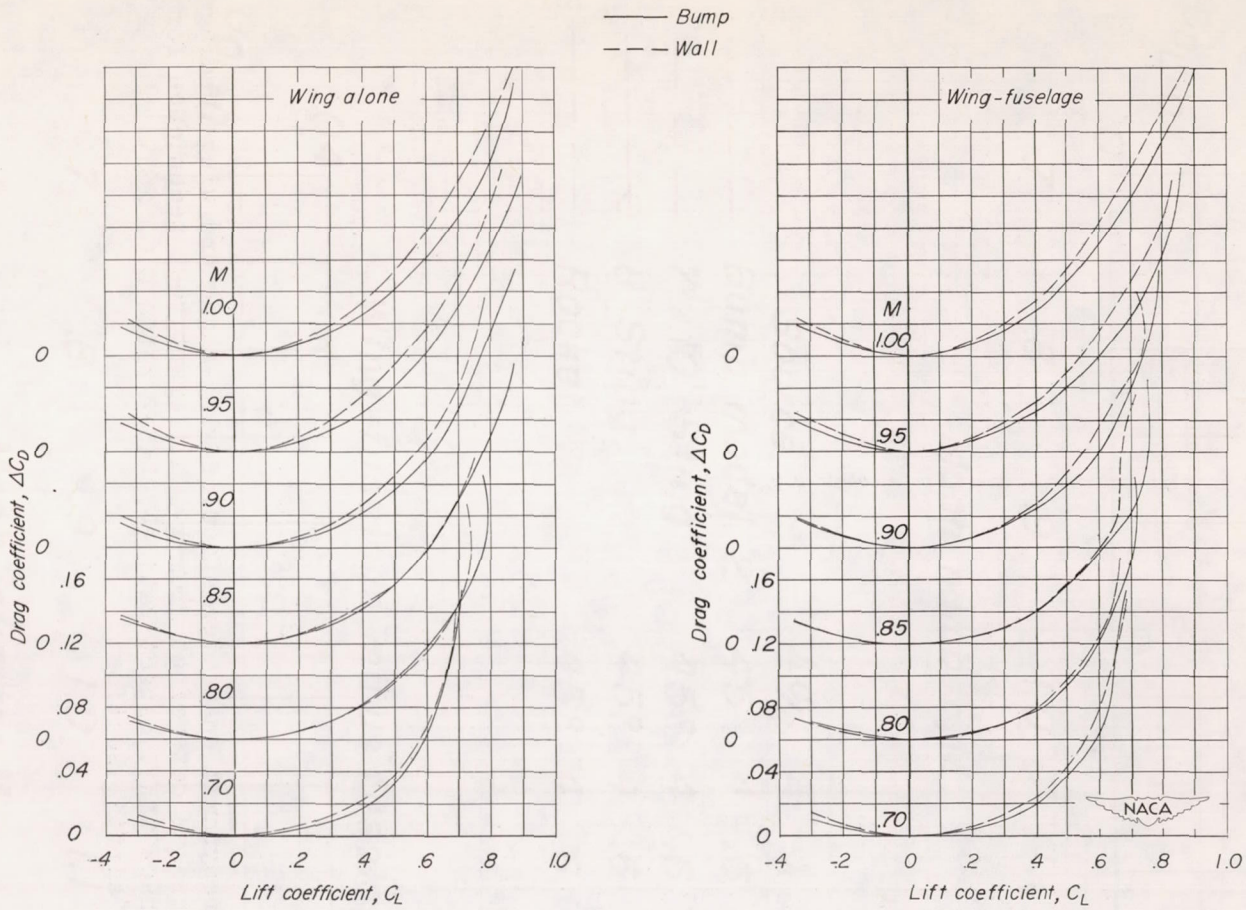

(c) C_D against C_L.

Figure 19.- Concluded.

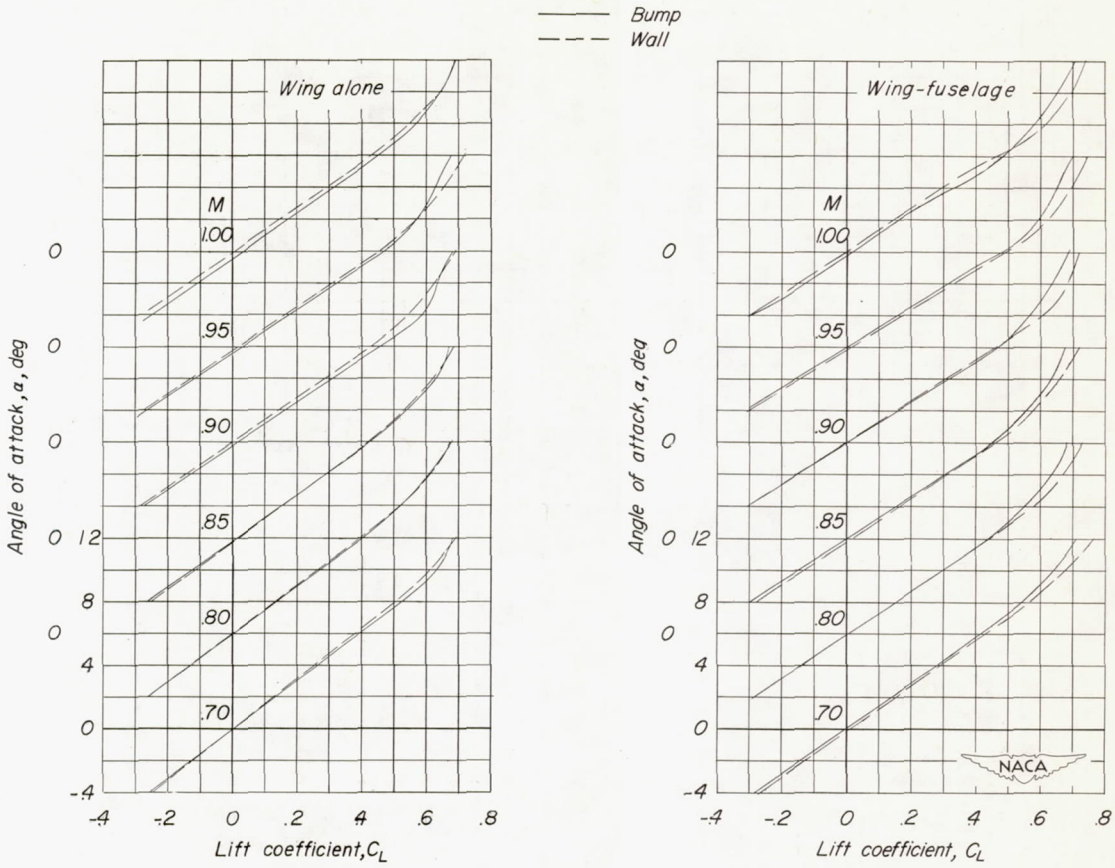

(a) α against C_L.

Figure 20.- Aerodynamic characteristics of wing-alone and wing-fuselage configurations as determined from two different test techniques for a 45° sweptback wing, aspect ratio 4, taper ratio 0.6, and NACA 65A006 airfoil section.

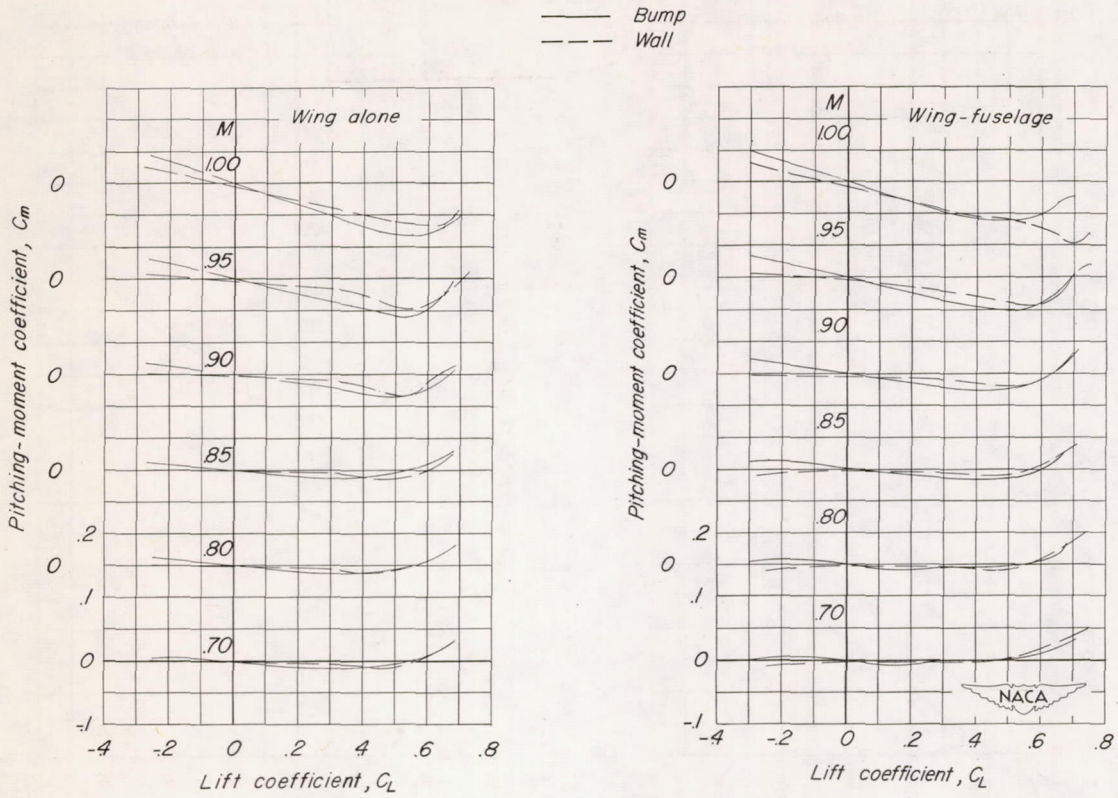

(b) C_m against C_L.

Figure 20.- Continued.

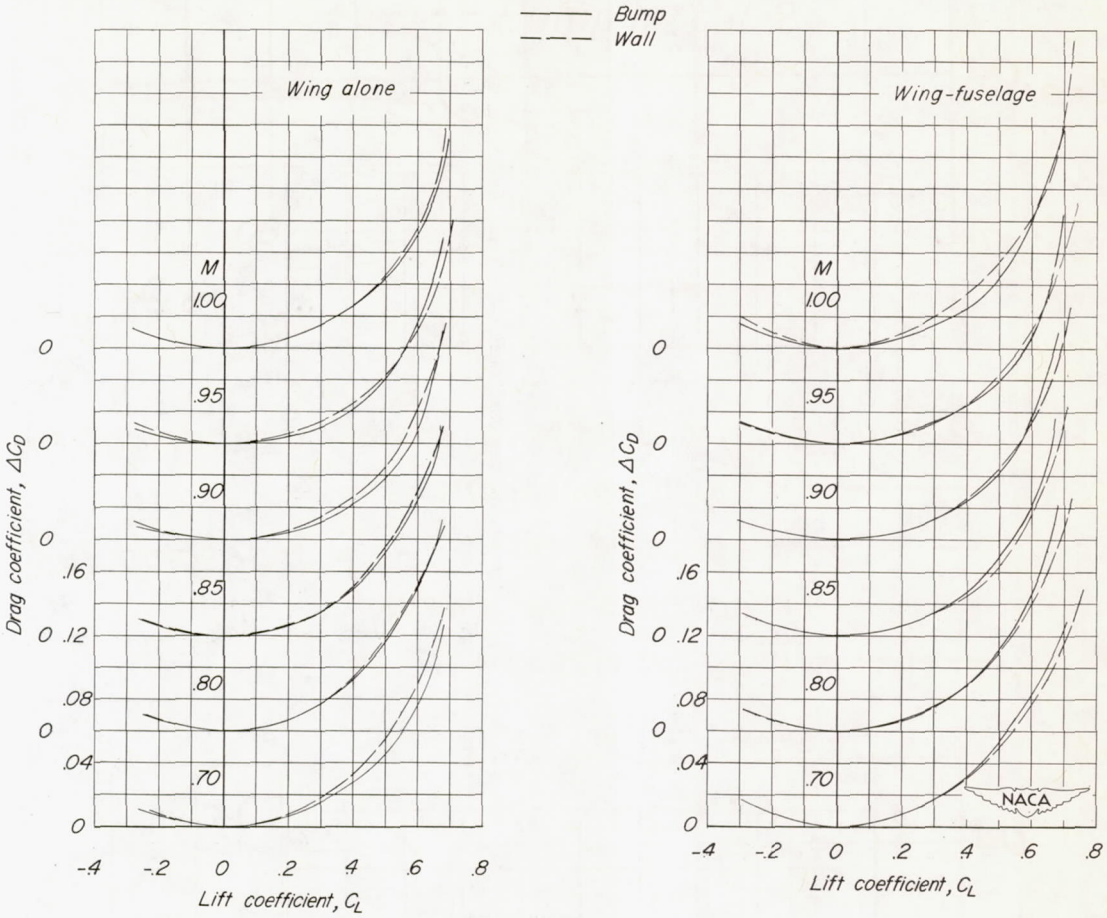

(c) C_D against C_L.

Figure 20.- Concluded.

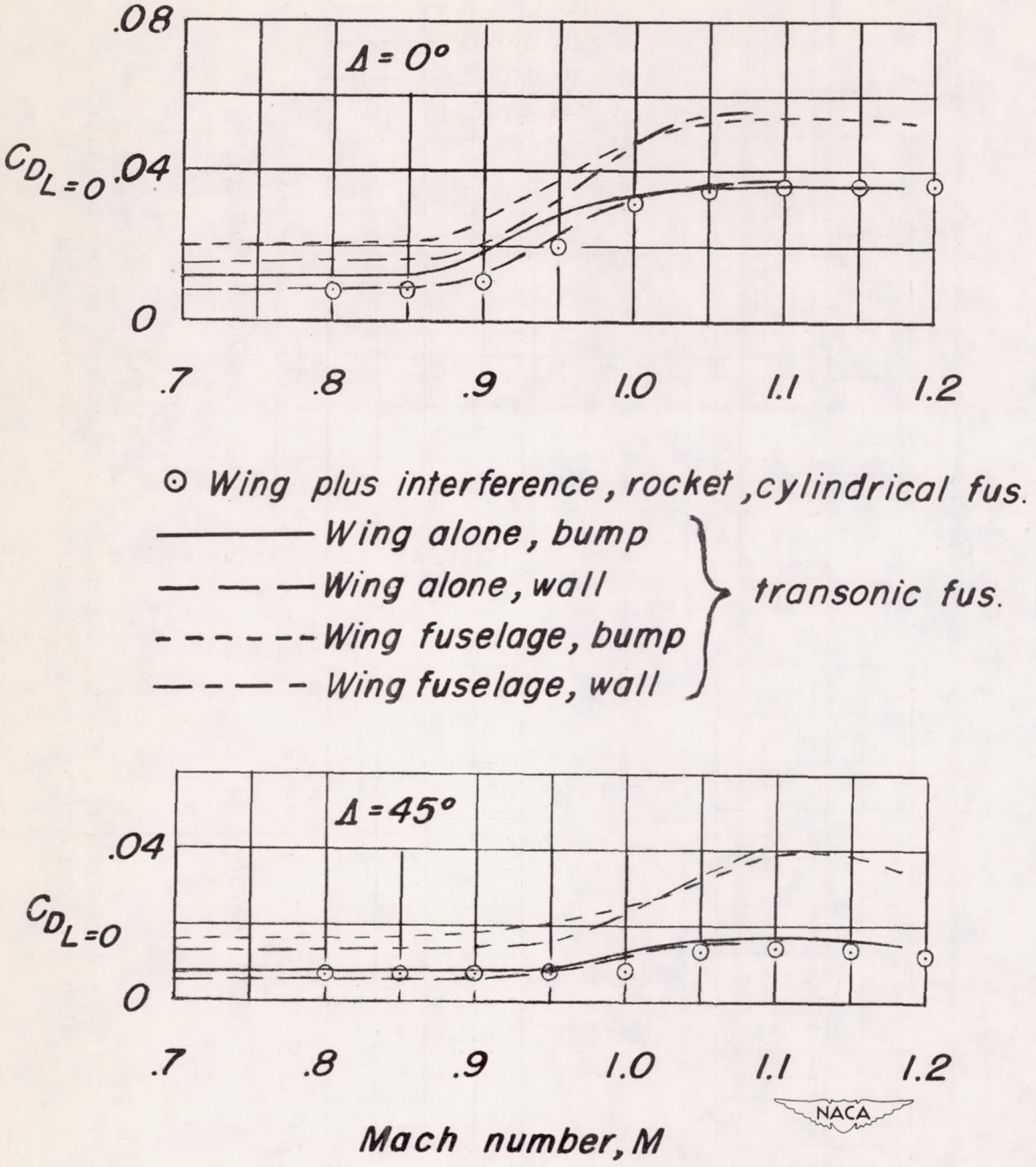

Figure 21.- Effect of sweep on the variation with Mach number of drag at zero lift for two test techniques and for two configurations.

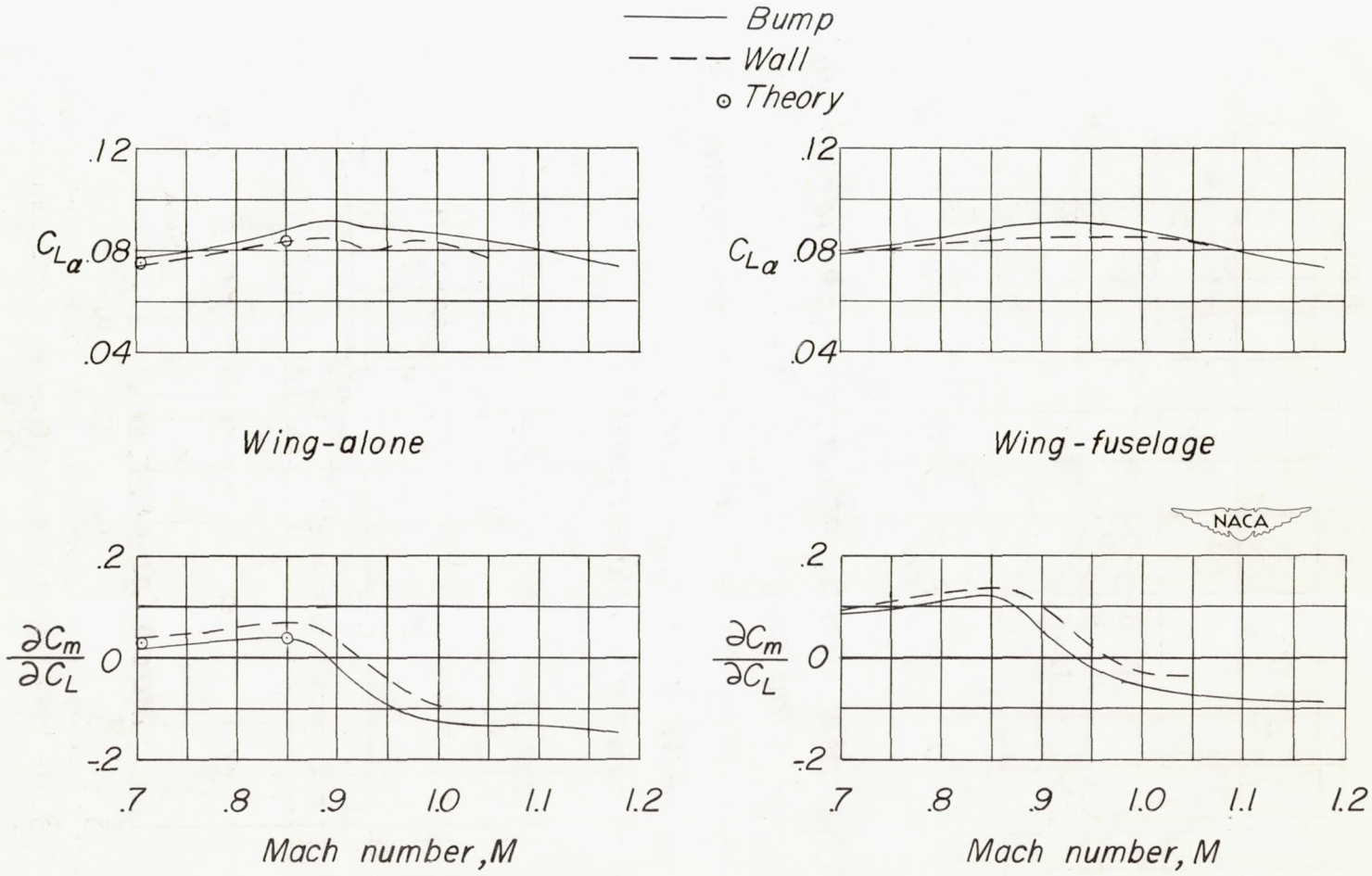

(a) $\Lambda = 0^{\circ}$.

Figure 22.- Variation of lift-curve slope and aerodynamic-center location with Mach number for two configurations at two sweep angles.

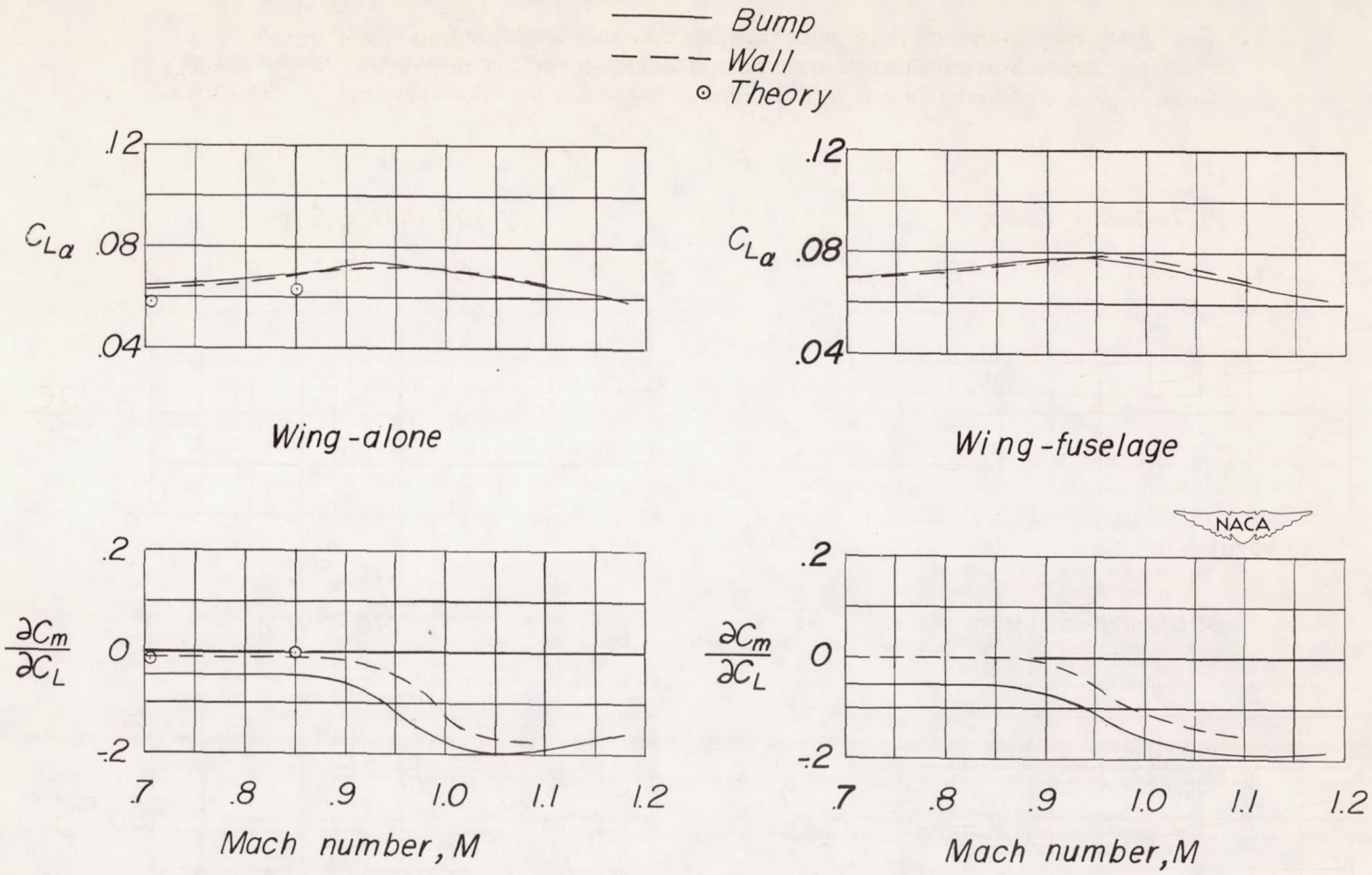

(b) $\Lambda = 45^{\circ}$.

Figure 22.- Concluded.

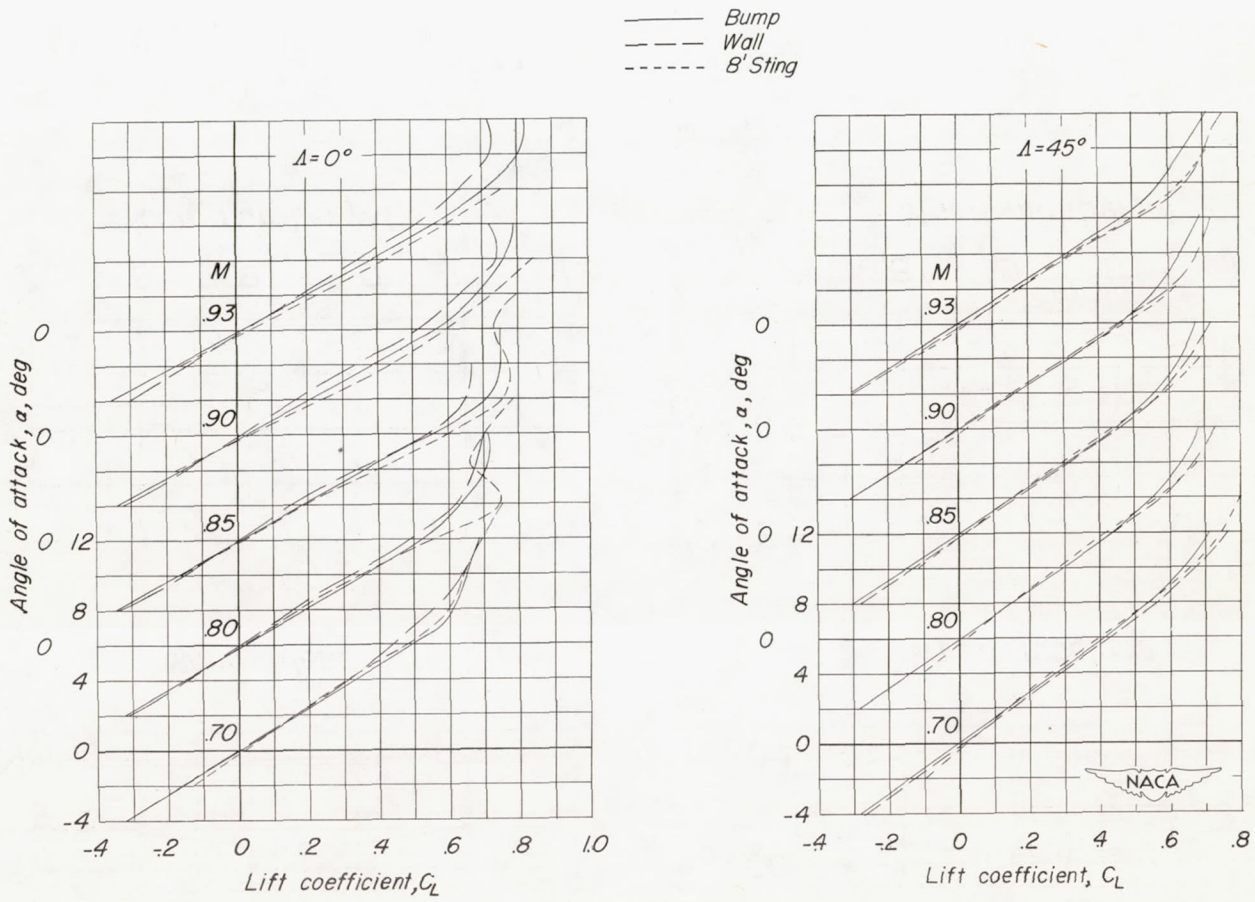

(a) α against C_L.

Figure 23.- Aerodynamic characteristics of two wing-fuselage configurations as determined from three different test techniques for an unswept and 45° sweptback wing, aspect ratio 4, taper ratio 0.6, and NACA 65A006 airfoil section.

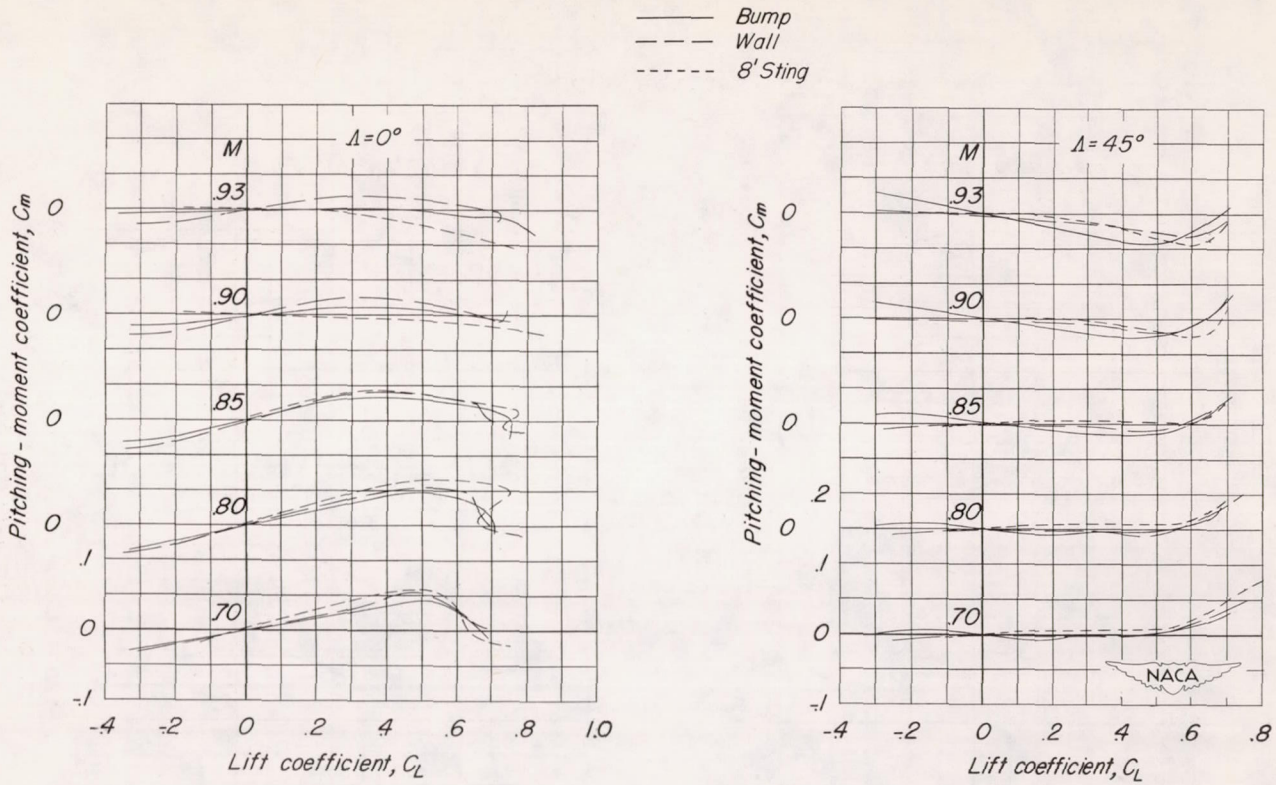

(b) C_m against C_L.

Figure 23.- Continued.

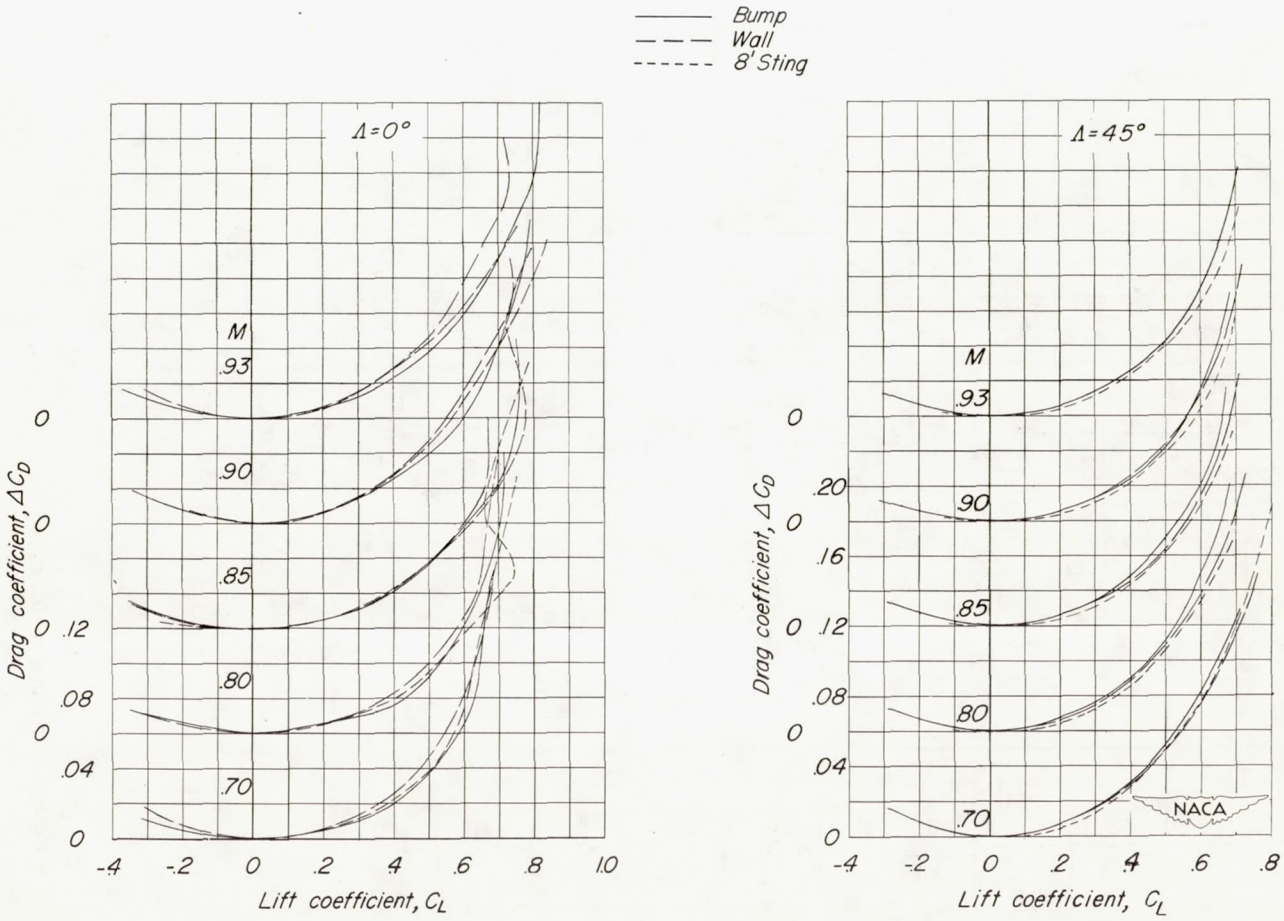

(c) ΔC_D against C_L.

Figure 23.- Concluded.